AUJUS

Auburn University Journal of Undergraduate Scholarship

Table of Contents

About the **Editors**

Paul Bergen is a senior studying Microbiology and German. His research focuses on searching for antibiotics from unculturable microorganisms in soil using molecular genetic techniques and describing the purified antibiotic compound. Paul is involved in Delta Phi Alpha, the National German Honor Society, the Microbiology Club, and the Auburn Mock Trial. He is also an Associate Justice on Student Government Association's judicial branch.

Emily Brennan is a senior studying Animal Science. She is a recipient of the Barry M. Goldwater scholarship awarded to undergraduates in the sciences for outstanding potential in their field. Her research explores the maternal transfer of antibodies in the House Finch and the retinal gene expression in chickens. Emily is president of the College of Agriculture Ambassadors and is a member of the Rowing Club.

Ragan Hart is a senior studying Exercise Science. As an AU Undergraduate Research Fellow, she worked in the Department of Kinesiology's Thermal Lab to study ankle-icing treatment. Ragan interned with the National Institutes of Health in summer 2011, and is interested in genetic epidemiology research in public health genetics, particularly obesity-related diseases and health issues.

Katherine McNair is a junior studying Mathematics and Sociology. She is currently preparing a research article for publication on the issue of technocracy, and is interested in finding new solutions to complex social problems through research on human rights. Katherine is the Officer for Public Relations for AU Students for Life.

Grace Moss is a senior studying English Literature. She is currently working on her Honors undergraduate thesis which focuses on drawing parallels between witchcraft and the presence of the supernatural in British Romanticism using the works of Samuel Taylor Coleridge. Grace is president of the Environmental Awareness Organization.

Hunter Rogers is a senior studying Chemical Engineering. His research focuses on ways to use nanotechnology in biomedical applications. Currently, he is studying how the shape, size, and magnetic characteristics of nanoparticles influence their use as imaging agents. Hunter is the Student Government Association's Assistant Director of Undergraduate Research and president and founder of the Tiger Think Tank, a student organization focused on research.

AUJUS Advisory Board

Daphni Green Advisor for Student Programs, Student Affairs

James Hansen Professor, History (former Director of Honors College)

Ross Heck Professor, Graphic Design

Jay Lamar Director, Pebble Hill Center for Arts and Humanities

Leanne Lamke Professor, Human Sciences

Amy Hecht Macchio Vice President for Student Affairs

Bonnie MacEwan Dean, Libraries

Carl Pinkert Associate Vice President for Research

Co-Editors in Chief

Margaret J. Marshall Director, Office of University Writing

Lorraine W. Wolf Director, Undergraduate Research

Letter from the **Provost** and the **V. P. for Research**

AUJUS

We are pleased to applaud the first issue of the *Auburn University Journal of Undergraduate Scholarship (AUJUS)*. With this new publication, Auburn takes a step forward in recognizing the academic and creative excellence of our undergraduate students. Undergraduate research offers our students an educational experience beyond the classroom. It combines the disciplinary knowledge and research expertise of our faculty with the creative intuition and enthusiasm of our best students.
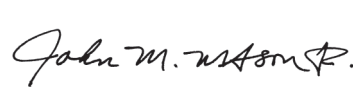
This publication's successful creation results from the hard work of the student editorial staff and production team. Without their perseverance and commitment, this volume would not have emerged. Students participating in the journal's production benefit from seeing the review process from the inside and from experiencing the complete cycle of the research experience.

The articles contained in this issue represent only a small subset of our students' diverse intellectual endeavors and accomplishments. None of this research would have been possible without the commitment of our faculty to educating the next generation of scholars. We express our deepest appreciation for the faculty's efforts to extend our institution's research culture to our undergraduate students.

We hope this volume will inspire readers to support and participate in the research process. Although often faced with obstacles, and sometimes failure, students involved in research learn that success is the result of perseverance, hard work, and creative passion. Please join us in congratulating these student authors on their publication success.

Timothy Boosinger
Interim Provost and
Vice President for Academic Affairs

John M. Mason, Jr.
Vice President for Research

Letter from
AUJUS
Editors-in-Chief

We are pleased to offer this inaugural issue of the Auburn University Journal of Undergraduate Scholarship (*AUJUS*). *AUJUS* grew from the collective vision of a few campus leaders dedicated to promoting undergraduate scholarship to a reality through the hard work of the undergraduate students themselves. The articles showcased in this first issue represent only a fraction of the impressive efforts of undergraduate students and their faculty mentors on the Auburn University campus. The scholarly and creative activity represented by these peer-reviewed papers demonstrates the extraordinary potential of Auburn students and we're very pleased to have been a part of this new venture.

Why is this publication so important? *AUJUS* provides our students with a professional outlet for their intellectual achievements not often available to students in their brief undergraduate careers. The selected articles clearly demonstrate that undergraduate students can make original, important scholarly contributions to their disciplines.

The opportunity *AUJUS* provides would not be possible without the tireless efforts of the student associate editors and the production team, the thorough and thoughtful comments of those who reviewed the articles, and the patience and professionalism of the student authors who persevered through the review cycle. Making it through these challenges is a "test" that validates the soundness of scholarly research and places it before the broader community for review. Research that has not withstood this test is research unfinished.

We look forward to the future with excitement and invite students from all disciplines to contribute their original research and creative scholarship to our next issue.

Lorraine W. Wolf
AUJUS Editors-in-Chief

Margaret J. Marshall

ABOUT THE COVER

Gabrielle Bates

Imagine a photography class in which you are required to produce images using all photographic elements… except the camera. That is what Professor Ross Heck, who has been teaching at Auburn for 26 years, told his class of graphic design students in the summer of 2011. The cover design for the inaugural issue of *AUJUS* evolved from this unconventional photography assignment that encouraged students to think outside the box to create truly unique images.

"It was a very experimental approach to image making," said Heck. "The interesting part of the class was that there was no failure." The graphic design students took the creative freedom in stride, employing all sorts of objects to create their images: candy, gelatin, dried flowers–even their own hair. Some students created photograms by placing objects directly on photographic paper, while others used laptop scanners to capture images.

Lauren Thompson created her image by using glitter and sand she found on the ground outside of the Wallace building. Lauren views the creative process as a fluid series of trial and error. "I try to look to things around me to inspire projects. I knew that I wanted to go for a celestial feel, so it was just a matter of finding the right materials to suit the project and playing around until I got a composition that I liked," she said.

Professor Heck described another one of his students, Rachel Botts, as someone who is "creative and sees the whole picture." By including banners and subtext in front of her photogram image, she created a cover design that clearly addressed the diverse nature of scholarly articles.

Gina Roberson made sure to incorporate both a scientific feel and Auburn appeal into her design. She created her cover design by editing a photogram she made by placing sand and a roll of masking tape onto photosensitive paper, applying light exposure, and then developing it in the darkroom. Gina tweaked the color scheme and edited the resulting image using Photoshop™, choosing orange and blue "to make the image more relatable to Auburn University."

Faced with these interesting and unique designs, the Editorial Board had a difficult decision to make. After much deliberation, the board members decided on a fusion between elements of two designs, juxtaposing Gina's vibrant and eye-grabbing image with Rachel's versatile layout. According to *AUJUS* Chief Editor Dr. Lorraine Wolf, Rachel's reusable layout showed impressive foresight and Gina's image "best captured the Auburn spirit."

While there is not always a research component to graphic design courses, Heck and his students have presented their own version of creative inquiry through a "critical lens." The *AUJUS* cover design represents both the creative thinking and intellectual awareness integral to the world of undergraduate research. Showcasing such work is at the heart of the *AUJUS* mission.

Fig 1a. Bone fragments showing active PH.

Fig 1b. Bone fragments showing healed PH.

CHILDHOOD HEALTH AND NUTRITION AT THE AUSTIN SITE (22TU549), TUNICA COUNTY, MS:

A BIOARCHAEOLOGICAL COMPARATIVE ANALYSIS OF SKELETAL REMAINS FROM VILLAGE AND MOUND CENTERS IN NORTHWEST MISSISSIPPI

Rachel M. Perash,
J. Alyssa White,
Kelsey E. Herndon,
Danielle N. Cook
and Kristrina A. Shuler

4

ABSTRACT

In this paper we analyze health patterns associated with the Mississippianization of a village site in the southeastern U.S. The Austin Site (22TU549), located in Tunica County, Mississippi, dates to approximately A. D. 1200. Archaeologists have traditionally been inclined to favor mound centers and overlook village sites due to a higher concentration of artifacts in the former. Thus there is a need to analyze smaller polities in order to contribute to a greater understanding of Mississippian culture. Past research has shown that mound centers typically have larger population densities and an increased reliance on agriculture, which may have contributed to poor nutrition among inhabitants. We argue that poor health caused by insufficient nutrition would have been less prevalent at the Austin village site than at mound centers because the population would have been smaller, and because a more balanced diet was possibly maintained through hunting and gathering rather than dependence only on agriculture. This paper analyzes childhood health patterns at Austin through observation of porotic hyperostosis, linear enamel hypoplasias, and stature of skeletal remains. We examined 61 individuals for these markers and found 53% (n=20) had porotic hyperostosis, 73.9% (n=17) of adults had linear enamel hypoplasias, and calculated stature averages of 164.4 cm for adult males. Comparison of Austin inhabitants to a nearby village (Bonds) and three mound centers (Humber, Lake George, and Mount Nebo) demonstrates relatively higher porotic hyperostosis and linear enamel hypoplasias at Austin but with reduced stature. The results of this small study suggest that Austin individuals may have suffered more often from poor nutrition during developmental years, but there was little difference overall between village and mound centers with regard to general indicators of childhood nutrition.

INTRODUCTION

The transitional period between Woodland and Mississippian cultures in the United States, roughly A. D. 400 to 1200, is often marked by a conversion of inhabited villages to overly populated mound centers. These mound centers usually serve as religious or political hubs. Often accompanying this transformation is a decline in nutrition accompanied by an increase in infectious diseases (*Goodman et al., 1984*). The introduction of poor nutrition and disease during a child's growth and development can have a significant impact on skeletal and dental growth and maturation rates. Poor childhood nutrition can present itself through observable generalized markers of health in the skeleton, the residual effects of which may remain into adulthood, especially if circumstances are not improved (*Larsen,* 1997; *Steckel and Rose, 2002*). Comparisons of various markers within and between sites allow for inferences regarding the associations of health status to population density and subsistence economies at village sites and mound centers.

We examined three types of health markers: porotic hyperostosis, linear enamel hypoplasias, and stature at the Austin village site (22TU549), located in Tunica County, Mississippi. Austin spans the Woodland-Mississippian transition and dates to circa A. D. 1200, according to radiocarbon dating (*Ross-Stallings, 2007*). The site was discovered by a plantation owner who had begun leveling pieces of land in 1988. Even though salvage operations were conducted, approximately a quarter of the site was destroyed by the time archaeologists arrived. Excavations by Nancy Ross-Stallings uncovered 149 internments and 40 wall trench houses, which were arranged in clusters within two palisades and associated bastions (*Ross-Stallings, 2007*). These floodplains provide a resource-abundant area for successful habitation, with some of the most fertile and diverse land in the world. In addition to Austin, several contemporaneous village and mound sites have been identified archaeo-logically from this area and previously analyzed for health indicators. Sites include Bonds (Danforth, 2007), Humber (*Danforth, 2007*), Lake George (*Listi, 2007*), and Mt. Nebo (*Danforth, 2007*), and are compared to Austin here for potential patterned differences in childhood health between settlement types.

MATERIALS AND METHODS

Burials from the Austin site were analyzed at the University of Southern Mississippi's physical anthropology lab under the direction of Danielle N. Cook and Dr. Marie Danforth. The skeletal sample from Austin consists of 149 individuals. Only skeletons in good to excellent condi-tion (n=61) were chosen for analyses in order to maintain analytical integrity. Age and sex were determined using traditional standards outlined in Buikstra and Ubelaker (1994) by Danielle N. Cook. Analysis of childhood nutrition was based on three markers, each scored by an independent observer to eliminate the potential for interobserver error. Porotic hyperostosis was assessed by Rachel M. Perash, linear enamel hypoplasias was scored by Kelsey E. Herndon, and long bones were assessed for stature by J. Alyssa White.

POROTIC HYPEROSTOSIS

Porotic hyperostosis is commonly characterized by cranial vault lesions distributed over the parietals, frontal, and, in rare cases, the occipital bones (Figure 1). Many scholars have agreed that PH is related to anemia, in particular an iron deficiency (*Stuart-Macadam, 1992; Ortner, 2003*). Precolumbian populations in the American Southwest were found to have had a diet rich in iron, thus leading to less evidence of PH than similar populations with diets low in iron (*El-Najjar et al., 1975*). Therefore, porotic hyperostosis is generally considered to be a good indicator of a diet lacking in iron or generalized metabolic insult (*Walker et al., 2009*). We scored porotic hyperostosis in 38 individuals with complete or fragmen-tary skulls following Stuart-Macadam (1985) and recorded four degrees of severity and four variations of activity level (see Table 1).

Table 1. Porotic Hyperostosis (PH) degrees of severity and variations of activity level.

POROTIC HYPEROSTOSIS (PH)	
PH ACTIVITY LEVEL AND DESCRIPTION	DEGREES OF PH SEVERITY SCORE AND DESCRIPTION
0 ⦂ NOT PRESENT	1 ⦂ BARELY DISCERNIBLE PINPRICKS
1 ⦂ ACTIVE, DISTINCT SHARP-EDGED FORAMINA	2 ⦂ TRUE POROSITY AND GENUINE PINPRICKS
2 ⦂ HEALED, SMOOTHING OVER, POSSIBLE REMODELING FORAMINA	3 ⦂ POROSITY WITH COALESCENCE OF FORAMINA
3 ⦂ MIXTURE OF ACTIVE AND HEALED FORAMINA	4 ⦂ POROSITY WITH CORAL-LIKE THICKNESS

LINEAR ENAMEL HYPOPLASIA

Linear enamel hypoplasia, a condition present on dental enamel, is expressed as transverse lines or pitting due to a temporary cessation of enamel production by ameloblasts during tooth formation (Figure 2) (*Goodman and Armelagos, 1988; Hillson, 1979; Pindborg, 1982; Sarnat and Schour, 1941*). Linear enamel hypoplasias can be attributed to a plethora of etiologies, including disease, undernutrition, trauma and hereditary anomalies (*Goodman, 1988*). Episodes due to systemic metabolic stressors, such as disease and undernutrition, are of the most interest to bioarchaeological studies for their utility in reconstructing past health conditions (*Goodman, 1990*). These instances can be identified by their presence on multiple teeth at points representing the same age at formation, whereas less common hereditary anomalies occur on all teeth and trauma usually occurs on one tooth (*Goodman, 1990*). When grouped with the other factors of stature and porotic hyperos-tosis, instances of linear enamel hypoplasias are widely considered to be a good indicator of generalized childhood health that preserve well in archaeological contexts (*Larsen, 1997*).
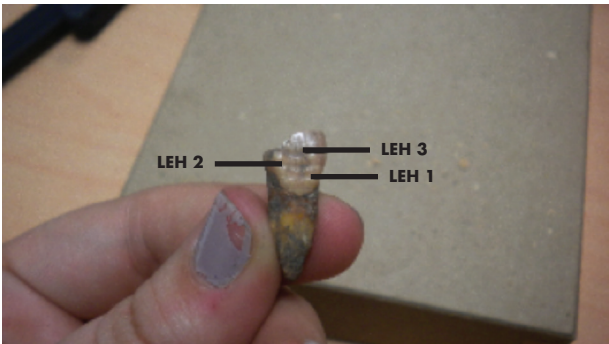

Fig 2. Illustration of LEH and how to measure LEH height on a tooth.

For this study, all mandibular canines and maxillary incisors were assessed using the fingernail test for presence or absence of linear enamel hypoplasias. Rates for the entire population, males, and females were calculated and compared with those of Bonds, Humber, Lake George, and Mt. Nebo.

STATURE

Stature, or terminal adult height, is often cited as a significant indicator of malnutrition with a positive correlation between caloric intake and growth velocity (*Auerbach and Ruff, 2010; Goodman and Martin, 2002*). Due to past studies that examined stature in relation to growth and nutrition, stature was calculated to provide supporting evidence for linear enamel hypoplasias and porotic hyperostosis results.

Tibia and femur maximum length measurements were taken from seven individuals using methods outlined in Standards (*Moore-Jansen et al., 1994*). Because of preservation issues, all samples were male. Stature calculations were then applied using regression formulae developed by Auerbach and Ruff (2010) for temperate populations of the prehistoric Southeastern woodlands using all intact femora and tibiae.

RESULTS

Our data collection and analysis of the Austin population culminated in the following results. We found that 53% of the population with skulls present had porotic hyperostosis. Of this 53%, 67% of males had porotic hyperostosis and 100% of females had porotic hyperostosis. The male population had an average stature of 164.4 cm. Finally, relatively

high rates of linear enamel hypoplasias were found at Austin at 73.9%. Of this 73.9%, 71.4% of males had linear enamel hypoplasias and 80% of females had linear enamel hypoplasias. The following charts (Figures 3, 4, 5) show the overall trends and data between the Austin, Bonds, Humber, Lake George, and Mt. Nebo sites.
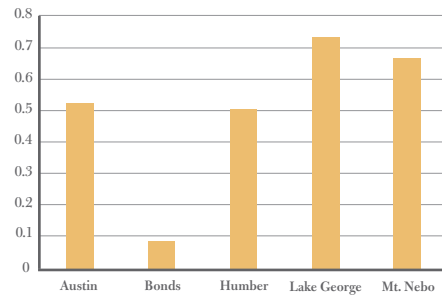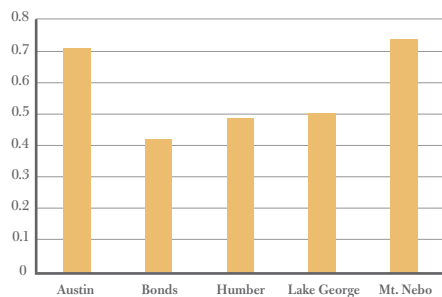

Fig 3. Average PH estimates (%) between compared sites.

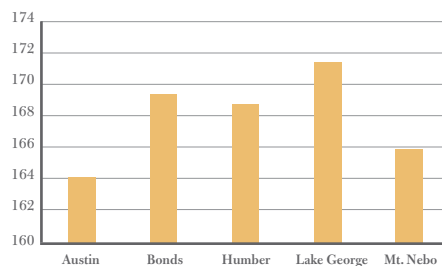**Fig 4.** Average LEH estimates (%) between compared sites.

Fig 5. Average stature estimates (in centimeters) between sites.

DISCUSSION

We were able to make a relatively cohesive statement about childhood health based on the combination of porotic hyperostosis, linear enamel hypoplasias, and stature. Childhood health at Austin was relatively poor in comparison to Bonds, Humber, Lake George, and Mt. Nebo. The data from Bonds differed from Austin in that the porotic hyperostosis and linear enamel hypoplasias levels were lower and the stature was higher. This trend of divergence was not what we expected considering that Austin and Bonds were both village sites in the Mississippian transitional period. Our original hypothesis expected Austin and Bonds to be similar, whereas we expected the data from mound centers to be distinct from these village sites. Instead, we discovered that Austin correlated more with the mound centers of Mt. Nebo in linear enamel hypoplasias and stature, with Humber in porotic hyperostosis, and was most dissimilar

from the village site Bonds in linear enamel hypoplasias and porotic hyperostosis and the mound center Lake George in stature as summarized in Table 2 .

The divergence between our expectations and results could be explained through the settlement conditions at Austin. Danforth (2007) discusses the possibility that the discrepancy between Austin and Bonds is likely caused by Austin's higher population density, which facilitated the transmission of infectious diseases and lessened access to resources. Village sites typically have lower population densities compared to mound centers. Similarities between mound centers (Humber, Lake George, and Mt. Nebo) and Austin can be attributed to pressures placed on the food supply and resource allocation due to their higher population density. Overall, Austin does not exhibit the trends of a typical village site and thereby offers an insight into the declining health associated with the transition of the Woodland to Mississippian cultural periods.

One common problem involved with any comparative study is the interobserver reliability for scoring and measuring. For porotic hyperostosis, the literature for Bonds, Humber, Lake George, and Mt. Nebo did not list where the porotic hyperostosis was observed, or only listed porotic hyperostosis on the occipital and/or parietal. This analysis took into consideration parietal, occipital, frontal, and temporal bones, a procedure that could result in higher porotic hyperostosis occurrence value for the individuals at Austin. Interobserver error also could have affected stature estimates since a more recent equation, which would not have been used in previous publications, was used. The equation applied to Austin individuals was specifically tailored to the southeastern region of the United States, while older studies may have used calculations based on nonspecific ancestry or a different combination of skeletal elements. Lastly, linear enamel hypoplasias were analyzed using mandibular canines and maxillary incisors. Comparative studies could have used different representational teeth that went unreported. If studies of the comparison sites had used teeth that were less susceptible to linear enamel hypoplasias, for example molars and premolars, then the end results would have been lower than that of Austin.

In addition to interobserver reliability, a small sample size could have prevented an accurate representation of the population at Austin. Of the original 149 internments, only 61 were chosen for analysis. The condition of bone, including taphonomic damage and natural growth appearance, may have affected an accurate evaluation of the overall population size. For these reasons, individuals available for assessment of porotic hyperostosis, linear enamel hypoplasias, and stature were greatly reduced. Even though preservation was acceptable, the majority of long bones were either broken or incomplete, thereby negatively affecting stature analysis. Among these 61, only five females were represented in the sample; therefore our results are not equally weighted between sexes.

Nevertheless, sites such as Austin and the associated villages and mound centers were ubiquitous in the late prehistoric Southeast. To this end, our study helps to

Table 2. An overall comparison of the five sites.

SITE	STATURE (CM) MALE	FEMALE	PH (%)	LEH (%)
AUSTIN (VILLAGE)	164.4	N/A	0.53	0.73
BONDS (VILLAGE)	169.5	161.2	0.09	0.44
HUMBER (MOUND)	168.9	160.0	0.51	0.50
LAKE GEORGE (MOUND)	171.5	164.8	0.74	0.52
MT. NEBO (MOUND)	165.8	134.1	0.67	0.75

bolster the available data on such settlements and the potential correlates between Mississippianization, population density, and childhood health. In addition, our data provide a basis for a future, large-scale analyses of Austin, or a larger study focused on the transition to agriculture in the Mississippi River Delta. Further research should include an examination of the remaining 101 internments from this site as well as a reanalysis of comparative sites using the same methodology to reduce interobserver bias.

CONCLUSION

Overall, Austin's combination of high levels of porotic hyperostosis and linear enamel hypoplasias coupled with short stature suggests these individuals had poor childhood nutrition. The childhood health of individuals at Austin, when compared to individuals from Mississippian mound centers and an earlier village site, may suggest that temporal and cultural periods are more significant to health than settlement patterns.

ACKNOWLEDGMENTS

REFERENCES

Auerbach, B.M. and C.B. Ruff. (2011). Stature estimation formulae for indigenous North American populations. *American Journal of Physical Anthropology*: 145 (1), 190–207.

Buikstra, J.E. and D.H. Ubelaker. (1994). *Standards for Data Collection from Human Skeletal Remains: Proceedings of a Seminar at the Field Museum of Natural History*. Fayetteville: Arkansas Archeological Report Research Series.

Danforth, M. (2007). Skeletal indicators of agricultural and economic intensification, in M.N. Cohen and M.M. Crane-Kramer (Eds.), *Ancient Health*. Gainesville: University Press of Florida, 65-97.

El-Najjar, M.Y., B. Lozoff, and D.J. Ryan. (1975). The paleoepidemiology of porotic hyperostosis in the American Southwest: Radiological and ecological considerations. *American Journal of Roentgenology*: 125 (4), 918-924.

Goodman, A.H., G.J. Armelagos, and J.C. Rose. (1984). The chronological distribution of enamel hypoplasias from prehistoric Dickson Mounds populations. *American Journal of Physical Anthropology*: 65 (3), 259-266.

Goodman, A.H. and G.J. Armelagos. (1988). Childhood stress and decreased longevity in a prehistoric population. *American Anthropologist*: 90 (4), 936-944.

Goodman A.H. and D.L. Martin. (2002). Reconstructing health profiles from skeletal remains, in R.H. Steckel and J. C. Rose (Eds.), *The Backbone of History Health and Nutrition in the Western Hemisphere*. Cambridge: Cambridge University Press, 11-60.

Goodman, A.H. and J.C. Rose (1990). Assessment of systemic physiological perturbations from dental enamel hypoplasias and associated histological structures. *American Journal of Physical Anthropology*: 33, 59–110.

Hillson, S. (1979). Diet and dental disease. *World Archaeology*: 11 (2), 147-162.

Larsen, C. S. (1997). *Bioarchaeology: Interpreting Behavior from the Human Skeleton*. Cambridge: Cambridge University Press.

Listi, G. A. (2007). Bioarchaeological analysis of diet and nutrition during the Coles Creek period in the lower Mississippi valley. Ph. D. dissertation. Department of Anthropology, New Orleans, LA: Tulane University.

Moore-Jansen, P.M., S.D. Ousely, and R.L. Jantz (Eds.). (1994). *Data Collection Procedures for Forensic Skeletal Material*. Knoxville: Forensic Anthropology Center, University of Tennessee.

Ortner, D.J. (2003). *Identification of Pathological Conditions in Human Skeletal Remains, Second Edition*. San Diego: Academic Press.

Pindborg, J.J. (1982). Etiology of development defects not related to fluorosis. *International Dental Journal*: 32, 123-134.

Ross-Stallings, N. (2007). Trophy taking in the central and lower Mississippi valley, in R. J. Chacon and D. H. Dye (Eds.). *The Taking and Displaying of Human Body Parts as Trophies by Amerindians*. New York: Springer Science and Business Media, 339-372.

Sarnat, B. G. and I. Schour. (1941). Enamel hypoplasias (chronologic enamel aplasia) in relationship to systemic diseases: Achronological, morphologic and etiological classification. *Journal of the American Dental Association*: 28, 1989-2000; 29, 67-75.

Steckel, R. H. and J. C. Rose (Eds.). (2005). *The Backbone of History: Health and Nutrition in the Western Hemisphere*. Cambridge: Cambridge University Press.

Stuart-Macadam, P. and S. Kent (Eds.). (1992). *Diet, Demography, and Disease: Changing Perspectives on Anemia*. New York: Aldine de Gruyter.

Stuart-Macadam, P. (1985). Porotic Hyperostosis: Representative of a Childhood Condition. *American Journal of Physical Anthropology*: 66 (4), 391-398.

Walker, P. L., R. R. Bathurst, R. Richman, T. Gjerdrum, and V. A. Andrushko. (2009). The causes of porotic hyperostosis and cribra orbitalia: A reappraisal of the iron-deficiency-anemia hypothesis. *American Journal of Physical Anthropology*: 139 (2), 109-125.

Walthall, J. A. (1990). *Prehistoric Indians of the Southeast: Archaeology of Alabama and the Middle South*. Tuscaloosa: University of Alabama Press.

Liposome-mediated transfer of mitochondria harboring foreign mitochondrial DNA into cultured fibroblasts

John Shi, Michael H. Irwin and Carl A. Pinkert

Abstract

The goal of this study was to use liposome-mediated transfer of mitochondria to create a stable cell line containing foreign mitochondria. In an earlier study we used fluorescence microscopy to demonstrate that mitochondria labeled with MitoTracker Red® CMXRos (Invitrogen, USA) can be transferred into cultured mouse NIH 3T3 fibroblasts using a commercially available, synthetic, unilamellar liposome formulation (Lipofectin®; Invitrogen, USA). In the present study, we used an improved liposome formulation, Lipofectamine® (Invitrogen), to transfer mitochondria harboring mitochondrial DNA (mtDNA) from one species of mouse, *Mus terricolor (M. terricolor)*, into 3T3 fibroblasts harboring mtDNA of the normal laboratory species of mouse, *Mus musculus domesticus (M.m. domesticus)*. We used species-specific PCR to show that transferred *M. terricolor* mtDNA was detectable within the cultured cells up to 3 weeks post-transfer. However, PCR analysis at 4 weeks post-transfer failed to detect the *M. terricolor* mtDNA, suggesting that the cultured cells selected against the transferred foreign mitochondria. In subsequent experiments we attempted to give transferred mitochondria a better chance for survival against selective pressures by partially depleting endogenous mitochondria with rhodamine 6G prior to the transfer of foreign mitochondria.

Introduction

Mitochondria are organelles that play a key role in cellular energy metabolism through oxidative phosphorylation (OXPHOS) and the production of ATP. Mutations in mitochondrial DNA (mtDNA) that negatively affect the function of oxidative phosphorylation enzyme subunits or mitochondrial protein translational mechanisms can result in severe impairment in tissues with high energy requirements (central nervous system, heart, skeletal muscle, etc.) (*Pinkert and Trounce, 2000; Cannon et al., 2011).* Our ultimate goal is to produce mouse models of human mitochondrial DNA disease. Toward this end, our lab is focused on development of technologies to introduce targeted mutations into mtDNA in isolated mitochondria *in vivo*, then to transfer these genetically altered mitochondria into living cells in culture. Previously, we demonstrated transfer of MitoTracker Red® CMXRos-labeled mitochondria into cultured mouse fibroblasts using synthetic liposomes *(Shi et al., 2008)*. Here, we show that *M. terricolor* mtDNA from liposome-transferred mitochondria was detected in cultured cells after several passages; however, the foreign mtDNA was only detectable for 3 weeks post-transfer, indicating that foreign mitochondria were eliminated. In an attempt to enhance retention of transferred foreign mitochondria, we then transferred mitochondria into cultured fibroblasts that were partially depleted of endogenous *M. m. domesticus* mtDNA by using rhodamine 6G (R6G) supplemented with uridine and pyruvate in the culture medium. Using the liposome-mediated transfer technique previously described *(Shi et al., 2008)*, isolated mitochondria from livers of xenomitochondrial D7 lineage mice *(McKenzie et al., 2004)*

"Proof that viable mitochondria can be stably transferred into cultured cells using synthetic liposomes will pave the way for adapting this technique"

harboring *M. terricolor* mtDNA were transferred into cultured fibroblasts. After passaging the transfected cells, a PCR assay with primers specific to *M.m. domesticus* and *M. terricolor* mtDNA was used to test for the presence of stable cell lines harboring *M. terricolor* mtDNA. Proof that viable mitochondria can be stably transferred into cultured cells using synthetic liposomes will pave the way for adapting this technique to transfer of genetically engineered mitochondria into cultured embryonic stem cells for development of live heteroplasmic mice that model human mtDNA diseases *(Pinkert and Trounce, 2007; Pinkert et al., 2010).*

Methods

Cells

The NIH 3T3 mouse fibroblast cell line was used for all experiments and cultured cells were maintained at 37°C in 5% CO_2 in air. Cells were plated onto 10 cm plastic culture dishes and grown in complete medium [Dulbecco's modified Eagle's medium (DMEM) containing 10% fetal calf serum (FetalClone® III; Hyclone, USA)]. For some experiments, when cells were approximately 80% confluent, the medium was changed to complete medium containing 0.7 µg/ml R6G and supplemented with sodium pyruvate and uridine. The medium was changed each day for 3 days. After 72 hours in R6G, the cells were allowed to incubate for 24 hours in complete medium without R6G.

Mitochondria

Mitochondria were isolated from livers of D7 xenomitochondrial mice harboring *M. terricolor* mtDNA *(McKenzie et al., 2004; Pogozelski et al., 2008)* as described previously *(Pinkert et al., 1997; Shi et al., 2008)*. Briefly, livers were dissected out and placed in ice cold SME buffer (250 mM sucrose, 10 mM MOPS, 1 mM EDTA, pH 7.4). Livers were minced and then homogenized with a glass Teflon® Dounce homogenizer in 30-40 ml of buffer. The homogenate was centrifuged twice for 10 minutes at 750 xg at

4°C, discarding pellets. The final supernatant was centrifuged at 9800 xg at 4°C for 15 minutes to collect mitochondria. Microsomes and blood pigments were removed from the pellet by vacuum aspiration, and the pellet was resuspended in STE buffer (250 mM sucrose, 50 mM Tris-HCl, 1 mM EDTA, pH 7.4) with a glass rod. Samples were re-homogenized with a glass-glass Dounce homogenizer and centrifuged at 9800 xg at 4°C for 15 min. After vacuum aspiration of microsomes and blood pigments, purified mitochondria were used for liposome encapsulation and transfer into 3T3 fibroblasts.

Liposome-mediated transfer

Isolated mitochondria were re-suspended with a glass rod in 250µl serum-free DMEM and 100µl were added to 100µl Lipofectamine® solution (20µl liposome stock solution plus 80µl medium, pre-incubated 30 minutes at room temperature). The mitochondria/Lipofectamine® suspension was incubated for 30 minutes at room temperature with gentle end-over-end mixing. One hour before transfer of mitochondria, complete medium was removed from cultured cells and replaced with serum-free DMEM. The liposome-encapsulated *M. terricolor* mitochondria were added to NIH 3T3 *M.m. domesticus* mouse fibroblasts in 10 ml of serum-free DMEM and incubated overnight (approx. 16 h) at 37° C in 5% CO_2. Control cells received either no treatment, mitochondria without liposomes, or liposomes without mitochondria. The next day, the medium was replaced with complete medium. Cells that were not pre-treated with R6G were passaged every 3-4 days (80-90% confluence) with aliquots of cells removed and used for DNA extraction and PCR analysis weekly for 4 weeks. R6G-treated cells that received mitochondria/liposomes were trypsinized and re-plated onto two 6-well plastic culture plates (samples 1-12 in *Figure 2*) to potentially enrich fractions of cells that took up the liposome-encapsulated mitochondria with greater relative efficiency.
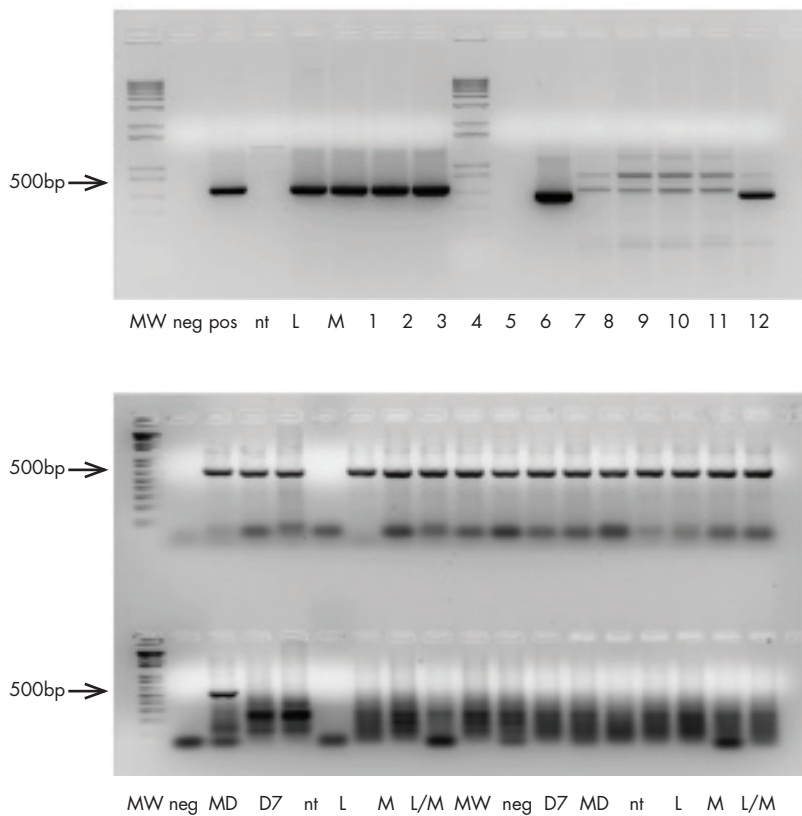
500bp →

MW neg pos nt L M 1 2 3 4 5 6 7 8 9 10 11 12

500bp →

500bp →

MW neg MD D7 nt L M L/M MW neg D7 MD nt L M L/M

Figure 1.
Liposome-mediated transfer of mitochondria into NIH 3T3 fibroblasts
Agarose gel of PCR analysis of total DNA from NIH 3T3 fibroblasts obtained 3 weeks post liposome-mediated transfer of foreign mitochondria containing *M. terricolor* mtDNA. **Left Panel:** PCR using primers specific for *M.m. domesticus* (endogenous) mtDNA shows a 550 bp amplification product. **Right Panel:** PCR using primers specific for *M. terricolor* mtDNA (from liposome transferred mitochondria). A 500 bp amplification product is indicative of foreign (transferred) mtDNA in cells treated with liposomes containing mitochondria from D7 xenomitochondrial mice (L/M). (MW, 100bp DNA ladder; neg, PCR negative control containing no template DNA; MD, *M.m. domesticus* control DNA; D7, control DNA from D7 xenomitochondrial line containing *M. terricolor* mtDNA; nt, 3T3 cells receiving no treatment; L, 3T3 cells receiving liposomes only; M, 3T3 cells receiving mitochondria only; L/M, 3T3 cells receiving liposome-encapsulated mitochondria)

Figure 2.
Liposome-mediated transfer of mitochondria into R6G treated NIH 3T3 fibroblasts
Agarose gel of PCR analysis of total DNA from R6G pre-treated NIH 3T3 fibroblasts obtained 2 weeks post liposome-mediated transfer of foreign mitochondria containing *M. terricolor* mtDNA. (MW, 100 bp DNA ladder; neg, PCR negative control; pos, PCR positive control: *M.m. domesticus* mtDNA for upper panel and *M. terricolor* mtDNA for lower panel; nt, 3T3 cells receiving no treatment; L, 3T3 cells receiving liposomes only; M, 3T3 cells receiving mitochondria only; 1-12 experimental R6G treated 3T3 cells that received liposome-encapsulated mitochondria). **Top row:** PCR of DNA from cultured 3T3 fibroblasts using primers specific for *M.m. domesticus* (endogenous) mtDNA showing a 550 bp amplification product. **Bottom row:** PCR of DNA from cultured 3T3 fibroblasts using primers specific for *M. terricolor* (transferred) mtDNA. Experimental samples (1-12) did not show the 500 bp amplification product of the transferred *M. terricolor* mtDNA.

PCR analysis

Total DNA was isolated from fibroblasts by phenol/chloroform extraction and ethanol precipitation. PCR was performed in 50μl reaction volumes using 50μg DNA with primers specific to D-loop sequences of mtDNA from *M.m. domesticus* or *M. terricolor* species. The amplification product using *M. m. domesticus*-specific primers was 550bp, while the amplification product using *M. terricolor*-specific primers was 500bp. Minimal cross reactivity was seen with *M. m. domesticus* primers; some cross reactivity was seen with *M. terricolor* primers, but was clearly distinguishable from the amplification product of the targeted sequence.

Results

These experiments were intended to show that isolated, viable mitochondria can be transferred into living cells using a commercially available liposome preparation that is routinely used for transfection of DNA into cultured cells. Development and optimization of this technique is an important first step for future experiments designed to perform targeted mutations of mitochondrial DNA *in vivo* prior to transfer of mitochondria into cultured cells.

In this report, we attempted liposome-mediated transfer of mitochondria containing mtDNA of a different species of mouse (*M. terricolor*) into NIH 3T3 fibroblasts containing mtDNA of the normal laboratory species of mouse, *M. m. domesticus*. Using a PCR assay that took advantage in sequence differences in the mtDNA between these two species, we were able to demonstrate liposome-mediated transfer of *M. terricolor* mtDNA into 3T3 fibroblasts after 3 weeks in culture post-transfer (*Figure 1*). *M. terricolor* mtDNA was not detected in samples from cells that received no treatment, mitochondria only, or Lipofectamine® only (*Figure 1*). After 4 weeks in culture, *M. terricolor* mtDNA was not detected in these cells (not shown), suggesting that the transferred mitochondria did not survive long in cells due to damage from the isolation procedure or were selected against in favor of endogenous mitochondria. To address the latter possibility, in separate experiments we treated cells with R6G for 3 days prior to liposome transfer of mitochondria. The R6G concentration we used was intended to deplete a large proportion (but not all) of endogenous

mitochondria in cultured cells, improving the chances for survival of transferred mitochondria, since they must compete with endogenous mitochondria for nuclear-encoded mitochondrial proteins. The R6G-treated cells, however, grew very slowly after liposome-mediated transfer and did not reach confluence until 2 weeks post-transfer. PCR analysis of total DNA from these cells at 2 weeks post-transfer showed the expected presence of endogenous *M. m. domesticus* mtDNA *(Figure 2, top panel)* but was unable to detect transferred *M. terricolor* mtDNA (*Figure 2, lower panel*). The DNA sample from control cells that received mitochondria only did not show an amplification product using either *M.m. domesticus* or *M. terricolor* PCR primers likely due to loss of the DNA pellet during ethanol precipitation and washing steps.

Discussion

The experiments presented here demonstrated that liposome-mediated transfer of mitochondria into cultured cells was effective in NIH 3T3 fibroblasts grown under normal conditions. Mitochondrial transfer into living cells represents a novel use for liposomes that has only been demonstrated by our laboratory. We were unable to detect transferred foreign mtDNA when cells were pre-treated with R6G to deplete endogenous mitochondria prior to liposome-mediated transfer. Hypothesized obstacles to effecting transfer of functional mitochondria in R6G-treated cells include: 1) possible residual amounts of R6G in cultured cells which destroyed transferred foreign mitochondria and 2) cultured cells may have been irreversibly damaged by the combination of R6G treatment and liposome treatment; thus only cells that did not receive significant amounts of liposome-encapsulated foreign mitochondria survived. Future research efforts will involve analytical studies dissecting foreign mitochondria transfer stability after treatment of cultured fibroblasts with R6G.

For nearly twenty years, methods for introduction of targeted mitochondrial modification have proven largely problematic (*Irwin et al., 2001; Pinkert et al., 2010*). A number of constraints were identified or postulated, from perturbations of biological pathways to mechanistic aspects of the specific protocols used (*Pinkert and Trounce, 2000; Pinkert and Trounce, 2007; Pinkert et al., 2010*). Since 1997, our laboratory has reported on methodologies used to create *in vivo* mitochondrial modifications in mammalian models (*Pinkert et al., 1997; Irwin et al., 1999; Irwin et al., 2001; Pinkert et al., 2010*). As such, ongoing research efforts will also target the mechanisms related to persistence of foreign mitochondria post-transfer. Such techniques hold significant promise in targeted modification of mitochondrial genes toward a new era in mitochondrial genetic therapy and future treatment options for afflicted patients.

References

Cannon, M.V., D.A. Dunn, M.H. Irwin, A.I. Brooks, F.F. Bartol, I.A. Trounce and C.A., Pinkert (2011). Xenomitochondrial mice: mitochondrial compensatory mechanisms, *Mitochondrion:* 11, 33-39.

Irwin, M.H., L.W. Johnson and C.A. Pinkert (1999). Isolation and microinjection of somatic cell-derived mitochondria and germline heteroplasmy in transmitochondrial mice, *Transgenic Research:* 8, 119-123.

Irwin, M.H., V. Parrino and C.A. Pinkert (2001). Construction of a mutated mtDNA genome and transfection into isolated mitochondria by electroporation, *Advances in Reproduction:* 5, 59-66.

McKenzie, M., I.A. Trounce, C.A. Cassar and C.A. Pinkert (2004). Production of homoplasmic xenomitochondrial mice, *Proceedings of the National Academy of Science USA:* 101,1685-1690.

Pinkert, C.A., M.H. Irwin, L.W. Johnson and R.J. Moffatt (1997). Mitochondria transfer into mouse ova by microinjection, *Transgenic Research:* 6, 379-383.

Pinkert, C.A., I.A. Trounce (2000). Production of transmitochondrial mice, *Methods:* 26, 348-357.

Pinkert, C.A., and I.A. Trounce (2007), Generation of transmitochondrial mice: Development of xenomitochondrial mice to model neurodegenerative diseases, *Methods in Cell Biology:* 80, 549-569.

Pinkert, C.A., L.C. Smith and I.A. Trounce (2010). Transgenic animals: Mitochondrial genome modification, *in* D.E. Ullrey, C.K. Baer and W.G. Pond (Eds.). *Encyclopedia of Animal Science,* 2nd ed., New York: Dekkar,Taylor & Francis, 1044-1046.

Pogozelski, W.K., L.D. Fletcher, C.A. Cassar, D.A. Dunn, I.A. Trounce and C.A. Pinkert (2008). The mitochondrial genome sequence of *M. terricolor:* Comparison with *M.m. domesticus* and implications for xenomitochondrial mouse modeling, *Gene:* 418, 27-33.

Shi, J., M.H. Irwin and C.A. Pinkert (2008). Liposome-mediated transfer of labeled mitochondria into cultured cells, *Ethnicity and Disease:* 18 (S1), 43-44.

$$\varepsilon_a = \frac{-c}{4} - \sqrt{\left(\frac{\mu_e + \mu}{2}\right.}$$

SIMULATIONS OF HYPERFINE SPECTROSCOPY OF ANTIHYDROGEN CONTAINED BY THE ALPHA COLLABORATION TRAP

PATRICK H. DONNAN AND FRANCIS ROBICHEAUX

ABSTRACT

We performed simulations of microwave spectroscopy of antimatter hydrogen atoms contained within the Antihydrogen Laser PHysics Apparatus (ALPHA) Collaboration trap. The microwaves cause transitions between the hyperfine levels within the ground electronic state. We launched an antihydrogen atom from a cylindrical spatial distribution in a simulated ALPHA trap. We gave it a velocity from a Maxwellian distribution that models the antihydrogen atoms that are created in the plasma environment of the trap. We then exposed the antihydrogen atom to microwaves resonant with the energy level splitting present in the trap. We show that microwave spectroscopy can be performed on trapped antiatoms within an experimentally feasible timescale. We present results of the transition rate for a range of frequencies to show where the largest resonance occurs within the trap and give decay rates for that microwave frequency. We show that the first spectroscopic measurements of antihydrogen are possible within current experimental bounds.

INTRODUCTION

With the advent of trapped antihydrogen (Andresen et al., 2010) stringent tests of charge-parity-time (CPT) symmetry between matter and antimatter are now within experimental bounds; long-time trapping of antihydrogen (Andresen et al., 2011) allows for the decay of the trapped antiatoms to the ground state. In this paper, we examine how

microwave spectroscopy of the hyperfine splitting of ground state antihydrogen might be performed on antiatoms trapped in the ALPHA Collaboration trap. The ALPHA apparatus is one of three experimental set-ups currently located at the European Organization for Nuclear Research (CERN).

ALPHA APPARATUS

The mixing trap in the ALPHA apparatus is where the positron plasma is combined with the antiproton plasma and the formation of antihydrogen occurs. Both plasmas undergo several processes before entering the mixing chamber in order to cool and otherwise prepare them for the antihydrogen formation. These processes are described in Butler (2011).

Once the plasmas enter the mixing trap, they are subject to magnetic fields from three sources: a pervasive solenoidal magnetic field along the axis of the trap generated by an external superconducting magnet (~1 T in magnitude), a field generated by two mirror coils (of varying strength), and a field generated by an octupole (of varying strength). The mirror coils are each located ~137 mm from the trap center in opposite directions and the octupole surrounds the mixing trap. These three sources combine to create a magnetic minimum at the center of the trap with a potential energy well depth of ~0.5 K. The trap has thirty-five electrodes, of varying size, that can be used to create electric fields in the trap which can direct the positron and

$$\left(\frac{\mu_p}{\ } B\right)^2 + \frac{c^2}{4}$$

antiproton plasmas. The electrodes are located around the trap and are electrically isolated from one another. The trap is surrounded by an annihilation detector which records the number of annihilation events once the magnetic fields are turned off and the antihydrogen allowed to escape from the trap, allowing for t*the* counting of the number of trapped antiatoms once noise has been accounted for.

CPT SYMMETRY TESTS AND BARYON ASYMMETRY

Though C, P and CP symmetries have been found to be violated in certain processes *(see Wu et al., 1957, and Christenson et al., 1964)*, CPT symmetry has not been found to be violated in any known processes. Spectroscopic measurements on antihydrogen are a prime candidate for CPT symmetry tests as hydrogen spectroscopy is very well established. The hyperfine splitting is known to parts in 10^{12}. A violation of CPT symmetry could help shed light on why the observable universe is composed of matter (the so-called baryon asymmetry). This paper describes simulations of how ground state antihydrogen will respond to applied microwaves assuming no CPT violations occur in the hyperfine splitting.

THEORY

In order to perform spectroscopic measurements on the antihydrogen atoms in the trap, the positron must transition from a spin-down state to a spin-up state. This transition causes the antihydrogen atom to switch from a low-field seeking state (or trapped state) to a high-field seeking state (one that is attracted to the walls of the trap where the magnetic field is strongest and thus will annihilate within fractions of a second). This transition is caused by creating a resonant magnetic field where the transition can occur by introducing microwaves into the trap.

GROUND STATE OF THE HYDROGEN/ANTIHYDROGEN ATOM IN A MAGNETIC FIELD

In the ground state hydrogen/antihydrogen atom placed in a magnetic field there are interactions between the spins of the particles and the magnetic field and the hyperfine interaction between the spins themselves. A derivation of the eigenstates can be found in many

upper-level quantum mechanics texts; for an example of the derivation see the section on hyperfine splitting in Gasiorowicz (1974). Four eigen states are possible; in Dirac notation these states are $|a\rangle = -\sin\theta\,|\uparrow\downarrow\rangle + \cos\theta\,|\downarrow\uparrow\rangle$, $|b\rangle = |\uparrow\uparrow\rangle$, $|c\rangle = \cos\theta\,|\uparrow\downarrow\rangle + \sin\theta\,|\downarrow\uparrow\rangle$, and $|d\rangle = |\downarrow\downarrow\rangle$, using *a* through *d* for ease of reference. The first arrow describes the spin of the electron and the second arrow describes the spin of the proton. The energies of these states are given by:

$$\mathcal{E}_a = \frac{-c}{4} - \sqrt{\left(\frac{\mu_e + \mu_p}{2} B\right)^2 + \frac{c^2}{4}} \qquad \text{(Eq. 1a)}$$

$$\mathcal{E}_b = \frac{c}{4} - \frac{\mu_e - \mu_p}{2} B \qquad \text{(Eq. 1b)}$$

$$\mathcal{E}_c = \frac{-c}{4} + \sqrt{\left(\frac{\mu_e + \mu_p}{2} B\right)^2 + \frac{c^2}{4}} \qquad \text{(Eq. 1c)}$$

$$\mathcal{E}_d = \frac{c}{4} + \frac{\mu_e - \mu_p}{2} B \qquad \text{(Eq. 1d)}$$

Where C is the 21 cm line constant in joules, I_e and I_p are the electron and proton magnetic moments and B is the magnetic field strength. The magnetic field causes energy level splitting through the Zeeman effect. Microwaves become resonant when the energy level difference between two states is equal to the microwave energy at a specific magnetic field value. For a magnetic field of 1 T, slightly under trap magnitudes, the *ad* resonance frequency is ~28.753407 GHz and the *cb* resonance frequency is ~27.333001 GHz.

THE LANDAU-ZENER APPROXIMATION

The Landau-Zener formula can be used to determine approximate probabilities of one state crossing into another at resonance conditions. Resonance occurs when the energy difference in either state *d* and state *a* or state *b* and state *c* (which is a function of the strength of the magnetic field that the atom moving through due to the Zeeman effect) is equal to frequency of the microwaves multiplied by Planck's constant. There are only two state changes that are relevant to the experiment, both of which are the positron flipping its spin, hence only the *a* to *d* and *c* to *b* transitions are being mentioned. The spin of the antiproton can flip as well, but the apparatus will not run at microwave frequencies resonant with these transitions so they can be ignored. Further state changes can be derived (in which both spins flip), but these are strongly suppressed and are not relevant for the experimental microwave power.

>>>>>>

Given the generic Hamiltonian with *V* as a coupling parameter:

$$H = \begin{pmatrix} E_1(t) & V \\ V & E_2(t) \end{pmatrix} \qquad \text{(Eq. 2)}$$

The Landau-Zener approximation gives the transition probability to go from state 1 to 2 as:

$$P_{1\rightarrow 2} = 1 - e^{-2\pi\Gamma} \qquad \text{(Eq. 3)}$$

Where (in terms of the reduced Planck's constant and the energy differences between the states):

$$\Gamma = \frac{V^2}{h}\left(\frac{1}{\frac{d}{dt}|[E_1(t) - E_2(t)]|}\right) \qquad \text{(Eq. 4)}$$

The coupling parameter, *V*, of the Hamiltonian is determined by when a state crossing can occur, which is:

$$\Delta\varepsilon - \hbar\omega = 0 \qquad \text{(Eq. 5)}$$

Where $\Delta\varepsilon$ is the energy splitting between the states (either *c* to *b* or *d* to *a*) and ω is the microwave frequency. The coupling parameter is proportional to the microwave field strength times a simple combination of the proton and electron magnetic moments. Γ, however, is proportional to the square of *V*, which means that the transition probably is dependent of the intensity of the microwaves. Using this, a probability of flipping the spin each time the resonant magnetic field is crossed by the antihydrogen atom can be determined and computed in the simulations.

NUMERICAL METHOD

The equations of motion in each direction are:

$$F_x = \frac{\partial}{\partial x}\,\mu B \qquad \text{(Eq. 6)}$$

And F_y and F_z have the same equation form, with the *x* replaced by *y* or *z*, respectively. I is the antihydrogen magnetic moment and is the magnetic field magnitude.

A fourth-order, adaptive step size Runge-Kutta recipe is used to compute the differential equations of motion of each antiatom. For further treatment of this method, see Press et al., (1992).

In order to determine when the spin of the positron has a chance of flipping, each time the antihydrogen atom transverses from area of magnetic field above the resonant magnetic field to an area of magnetic field below the resonant field, the rate of the change must be known in order to compute the amount of time spent in the resonant regime and thus the probability of a spin flip (see Eqs. 2 and 3). Essentially, this means computing a slope of the motion (i.e., the velocity of the antihydrogen atom) in order to compute the change in energy present in coupling parameter. To do this, we used a Lagrange interpolating polynomial to construct a second order polynomial. The real roots of this polynomial were then found, and any roots between the previous time step and current step were treated as times of

$$F_x = \frac{\partial}{\partial x}\,\mu B$$

possible spin flips. The derivative of the polynomial gave the slope (i.e., velocity) at those times that could then be used to compute the probability of a spin flip. We used a Monte Carlo method for determining whether or not the spin flipped at each crossing. A Monte Carlo method was also used for determining if a noise count due to cosmic events occurred.

RESULTS

As discussed earlier, the transition probability depends on the strength of the applied microwaves. For all simulations, the microwave electric field strength was 200 V m^{-1}. This value is at the upper end of current experimental capacity. Electric field strength has a significant influence due to the scaling of the transition probability with the square of the coupling parameter. If the electric field strength is halved, the power and transition probability are decreased by a factor of four, which causes the time scale on which the experiment can be performed to be increased by a factor of four.

In order to cut down on the number of simulated noise counts caused by cosmic events only detection events that occurred with the center half of trap were counted. Because this is where the vast majority of the antihydrogen annihilation events occur, we found that this method should serve to improve the statistics in the experimental runs. Most annihilation events occur here because the only region where the microwaves are resonant with the magnetic fields occurs near the center of the trap, and the flipped antihydrogen is then directly attracted to the strong fields at the trap walls. The antihydrogen then ends up annihilating before enough time to move significantly along the trap axis has elapsed.

An important note is that these simulations assume an average trapping rate of one antihydrogen per run. Doubles or trebles of trapped antiatoms would lead to a significant reduction in the cosmic count to spin flipped antihydrogen count ratio, giving better statistics.

$$\Gamma = \frac{V^2}{h}\left(\frac{1}{\frac{d}{dt}|[E_1(t) - E_2(t)]|}\right)$$

PULSED MICROWAVE SIMULATIONS

We applied the microwaves using a pulse method. The pulse method involved turning on resonant microwaves at a frequency below any magnetic field present in the trap and leaving them on for a five second duration (which is within experimental bounds). After that duration, the microwaves are tuned to a new energy above the first but still below any magnetic field present in the trap and left on that frequency for the same duration. Then, the microwaves are tuned to a frequency which is resonant for a magnetic field present in trap (hence above the first two) and left on that frequency for the same duration. This is the first time that any spin flips can occur, and this means that any counts on the detector found before this duration are noise (i.e., cosmic) counts. Lastly, the microwaves are tuned to a resonant field above the third field and left to run for a fourth and final duration.

Initially, simulations were run starting with relatively large changes in frequency. Simulations were then progressively run with smaller changes in the frequency as the resonant frequency at the center of the trap was narrowed in on. It was found that setting the microwaves to be resonant right at the center of the trap gave the quickest decay rate in the number of antihydrogen remaining in the trap as a function of time (i.e., the unflipped antiatoms).

Figure 1 contains graphs of ten simulations of twenty-five runs containing a trapped antihydrogen atoms beginning the *c* eigenstate and transitioning to the *b* eigenstate, and the corresponding noise graph for these runs. Figure 2 contains the same results but for the *d* to a transition. The step size of the change in frequencies of the results displayed in this graph is one part per thousand of the resonant frequency at the center of the trap. The initial resonant frequency is fifteen parts in ten thousand below resonant frequency at the center of the trap, the second is five parts in ten thousand below, the third is five parts in ten thousand above and the last is fifteen parts in ten thousand above. Of note in both figures is the decreased number of flips during the last duration, which is due to most of the antiatoms having already flipped during the third duration. Antiatoms with higher kinetic energies are less likely to spend as much time around the center of the trap and thus are more likely to have flipped in the last microwave pulse.

The accuracy to which the magnetic fields in the trap must be known is thus on the same order as the frequencies (i.e., parts in ten thousand). This could provide difficulties to the experimental runs due to the challenge of measuring the magnetic fields in the trap. Uncertainty in magnetic field strength turns up in the uncertainty term in the spectroscopic measurement, so knowing the fields in the trap leads to more precise measurements in the spectroscopy.

Having two different transitions presents a potential problem if the resonant frequencies overlap at any point in the tested frequencies. Fortunately, if the pulses are based from the frequency resonant at the center of the trap and have a small enough change in frequency between them, there is no overlap between pulses for the two transitions. The size of this change is within experimental capacities, so this should not be an issue for the ALPHA experimentalists. No overlap also means that the noise from the runs for each transition can be treated separately and not considered statistically during the pulses for the other frequency. In the scenario, the experimentalists run the pulse sets back to back, first for the *c* to *b* transition (which has lower resonant frequencies) and then for the *d* to *a* transition (which has higher resonant frequencies).

TRANSITION RATE AS A FUNCTION OF MICROWAVE FREQUENCY

An advantage to running simulations as opposed to an actual experiment is the ability to test many different frequency resonances at once. In Figure 3, the transition rate as a function of frequency is given for both transitions. These simulations never actually flipped the spin but rather recorded probabilities to flip for a set of frequencies over a given time duration. This shows a profile of the best resonant frequencies to use in the experiment, i.e., which gives the maximum probability to flip over an arbitrary time duration. Of note is the relatively sharp decay of these curves. Within a change in frequency of ~100 MHz the rate has largely decayed. The sharper the curve the easier it will be, in principle, for ALPHA experimentalists to improve the precision of the spectroscopy.

$$\mathcal{E}_a = \frac{-c}{4} - \sqrt{\left(\frac{\mu_e + \mu_p}{2}B\right)^2 + \frac{c^2}{4}}$$

>>>>>>

Figure 4 shows the decay rate for the antihydrogen population when the microwaves are tuned to a frequency resonant at the center of the trap. This is what we found to be the sharpest decay rate possible in the trap. This can be seen by comparing Figure 3 to Figure 4: the resonant frequency at which the simulations that generated Figure 4 were run is the peak of the rate curve in Figure 3.

CONCLUSIONS

We have presented simulations of microwave spectroscopy of the hyperfine splitting in the ground state of antihydrogen. We used a pulsed application method to apply the microwaves; we have also presented the transition rate as a function of frequency and the decay rate for microwaves resonant with the center of the trap. These simulations show the hit and decay rates ALPHA experimentalists should see if there are no CPT symmetry violations in one precision measurement of antimatter given current experimental bounds. Once completed, these experiments will be able to give us the first spectroscopic look at antimatter and perhaps shed light on why we do not observe antimatter in the universe.

ACKNOWLEDGMENTS

REFERENCES

Andresen, G. B., et al. (ALPHA Collaboration). (2010). Trapped antihydrogen. *Nature*: 468 (7324), 673.

Andresen, G. B., et al. (ALPHA Collaboration). (2011). Confinement of antihydrogen for 1,000 seconds. *Nature Physics*: 7 (7), 558-564.

Butler, E. (2011). Antihydrogen Formation, Dynamics and Trapping. Ph. D. thesis. Department of Physics, Swansea, Wales, United Kingdom: Swansea University.

Wu, C. S., E. Ambler, R. W. Hayward, D. D. Hoppes, and R. P. Hudson. (1957). Experimental Test of Parity Conservation in Beta Decay. *Physical Review*: 105 (4), 1413.

Christenson, J. H., J. W. Cronin, V. L. Fitch, and R. Turlay. (1964). Evidence for the 2π decay of the $K2^0$ meson. *Physical Review Letters*: 13 (4), 138.

Gasiorowicz, S. (1974). *Quantum Physics* (1). New York: Wiley.

Press, W. H., S. A. Teukolsky, W. T. Vetterling and B. P. Flannery. (1992). *Numerical Recipes*. (2). New York: Cambridge University Press.

(a)

Annihilation Counts for the C to B Transition Using the Pulse Method

(b)

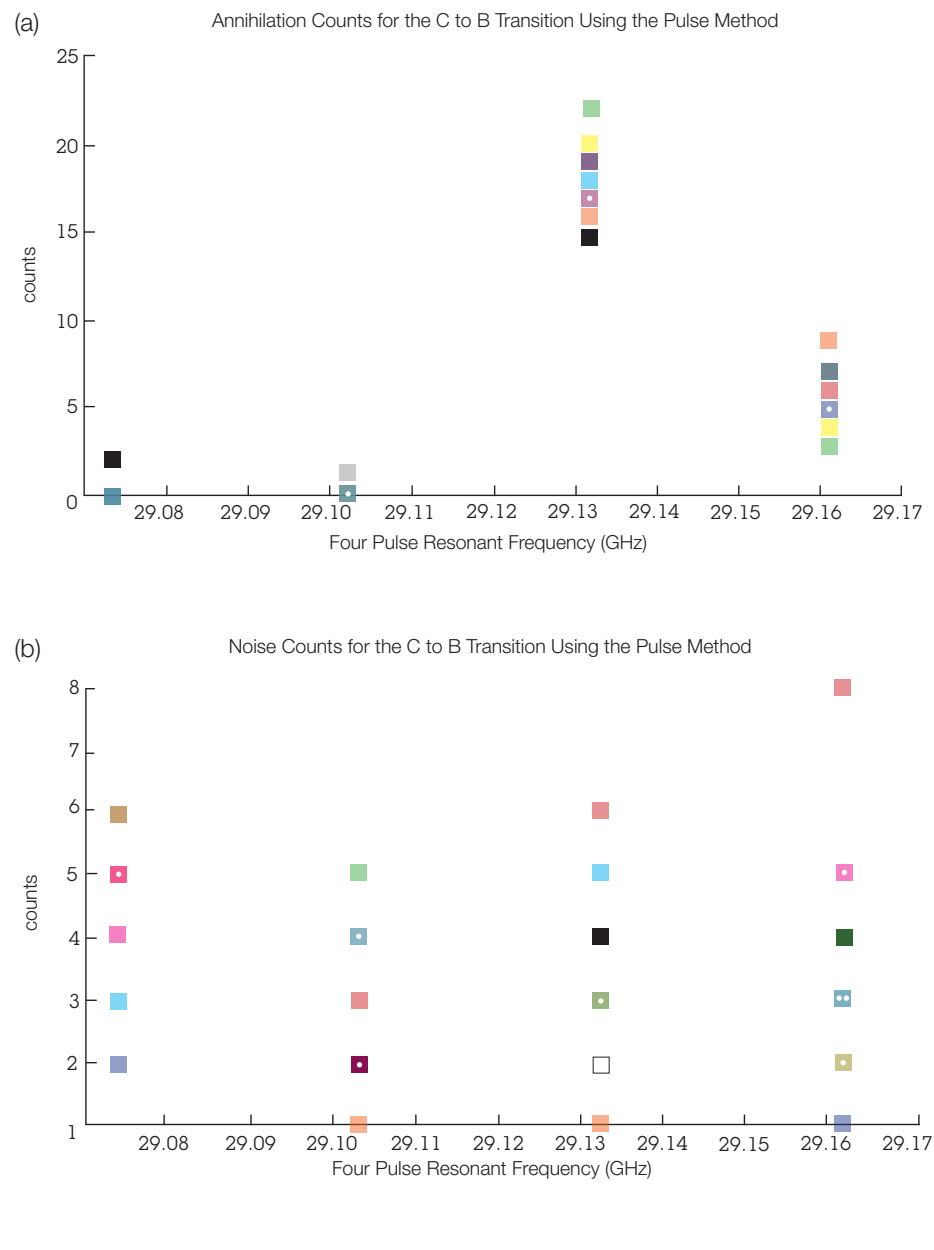**Noise Counts for the C to B Transition Using the Pulse Method**

Figure 1. This figure shows annihilation and noise counts for 10 simulations, each denoted by a set of points, of 25 successful trapping runs each. Each symbol, such as the green square and the white box, thus represents a statistically independent simulation. The spread shows the fluctuation expected over 10 sets of 25 trapping runs. Fig. 1a shows detection events due to actual spin flips of trapped antihydrogen; the Fig. 1b shows noise events detected throughout the simulations. These simulations were for a microwave electric field strength of 200 V m^{-1} and for antihydrogen in the *c* eigenstate (transitioning to the *b* eigenstate). Notice the difference in the *y*-axis scale between the two graphs.

(a)

Annihilation Counts for the D to A Transition Using the Pulse Method

(b)

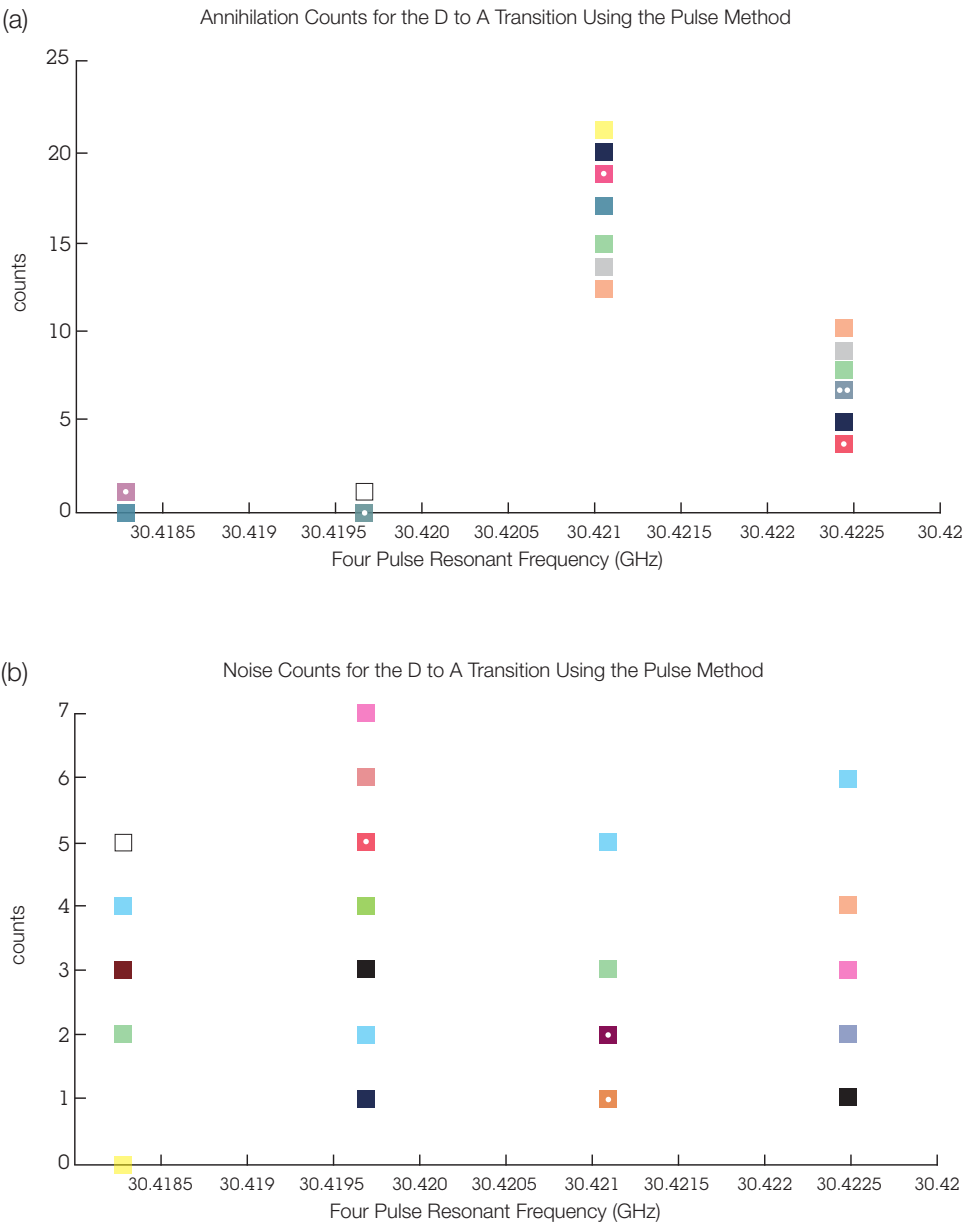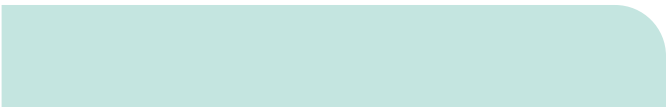### Noise Counts for the D to A Transition Using the Pulse Method

Figure 2: Same as Figure 1, but for antihydrogen starting in the *d* eigenstate, transitioning to the *a* eigenstate. Again, each set of points represents one simulation of 25 successful trapping runs.
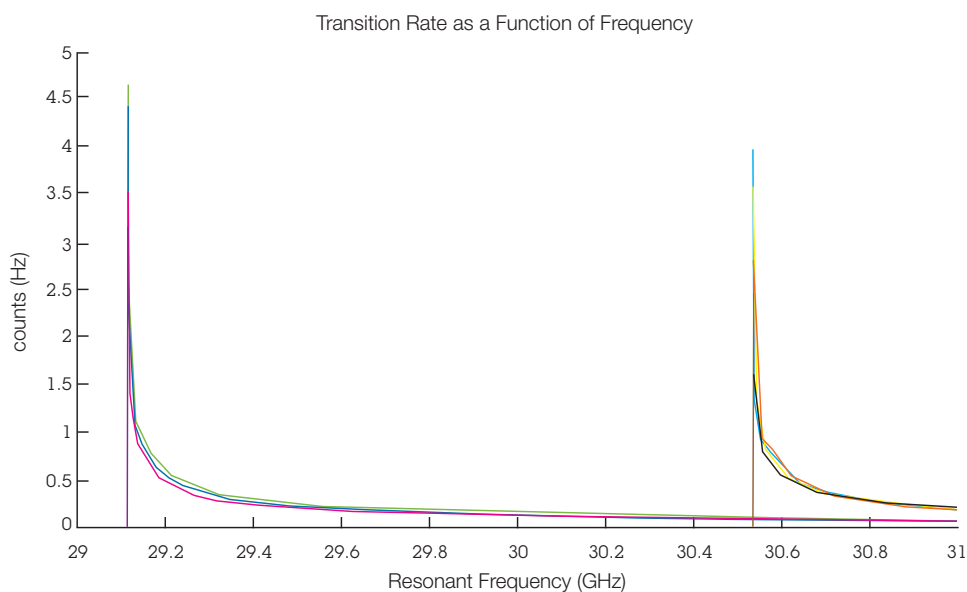
Transition Rate as a Function of Frequency

Figure 3: A profile of the resonance lines for each transition as a function of frequency. This graph shows curves generated from four simulations for each starting eigenstate at a microwave field strength of 163 V m⁻¹. The green, magneta, dark blue, and red lines begin in the *c* eigenstate and the orange, light blue, black and yellow lines begin in the *d* eigenstate. Notice the peaks are separated by a large enough amount that noise from each part can be separated (when using a pulse application method) when dealing with the experimental statistics.
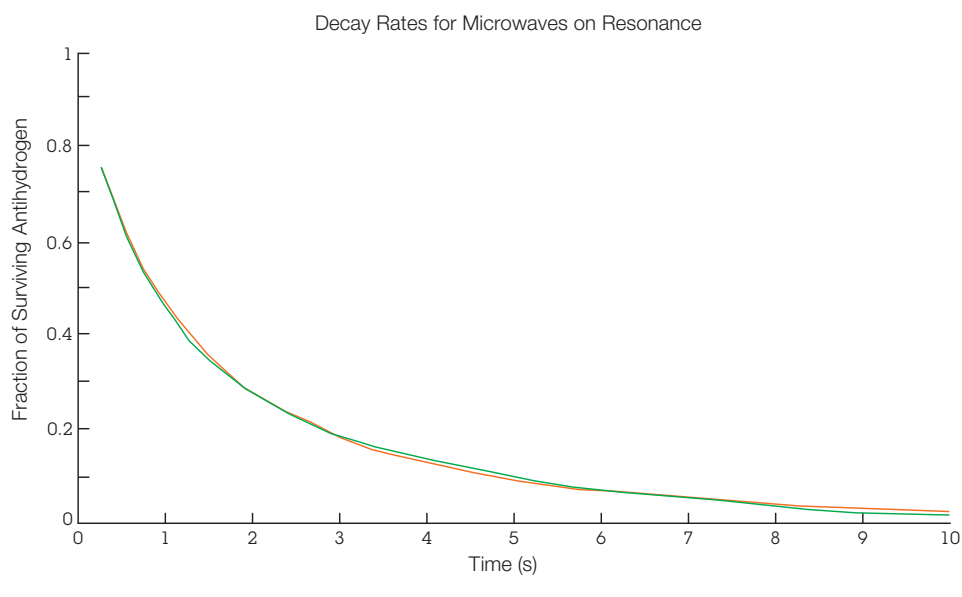
Decay Rates for Microwaves on Resonance

Figure 4: Decay rates for the survival probability of trapped antihydrogen when microwaves are applied resonant with the magnetic field at the center of the trap at an electric field strength of 163 V m⁻¹. The red line shows the *c* to *b* transition; the green line shows the *d* to *a* transition. These runs are run at the peak microwave values on Figure 3.

Molecular Photovoltaic Systems Based on Porphyrin/Fullerene Assembled in Lipid/Alkanethiol Hybrid Bilayers: A Preliminary Study on the Effect of the Thickness of Self-Assembled Alkanethiol Monolayers on Photocurrents

Bradley Lane Young and Wei Zhan

Abstract

Organic photovoltaic (OPV) devices promise to offer us inexpensive solar cells that can potentially alleviate our dependence on fossil fuels based energy sources. To further improve the performance of today's OPV devices, new materials as well as systematic studies of fundamental photoconversion processes and mechanisms are needed. Here, we report a multicomponent molecular photovoltaic system that is based on amphiphilic porphyrin/fullerene assembled in a hybrid phospholipid/alkanethiol bilayer. The final structure is immobilized on gold electrodes, which allows photocurrent generated from photoactive porphyrin and fullerene to be reliably followed. The important issue we will address here is the distance between photoactive agents to the electrode surface. Specifically, according to the classical electron transfer theories, the efficiency of electron transfer decays when the distance of electron exchange increases. The control of electron transfer distance is realized in this study by using n-alkanethiols, $CH_3(CH_2)_nSH$, where n=9,11,13,15 and 17, as the underlying layer in the hybrid bilayer structure.

Introduction

The ecosystem and once stable climate on Earth are experiencing a strengthening strain due to the continual rise in green-house gas emissions. Compelling scientific evidence has been collected that indicates the massive amount of fossil fuels consumed by humans is directly responsible for the spike in atmospheric CO_2. In order to counter such a negative trend, actions must be taken to reduce the amount of fossil fuels consumed and find new renewable energy sources at reasonable costs. While untapped oil reserves are predicted to last no more than 150 years, 60-160 years of natural gas reserves are estimated (*Lewis and Nocera, 2006*). Several potential alternatives, ranging from nuclear power to biofuels and hydro-/wind powers, have been suggested, but the most promising solution involves direct utilization of solar energy.

Novel solar light utilization mechanisms such as photovoltaics (PV) have the potential to shift our current energy generation/consumption paradigm from fossil fuels to an essentially inexhaustible source. For example, the amount of solar energy received by the earth per hour (4.3×10^{20}J) is more than all of the energy consumed by humans annually (4.1×10^{20}J) (*Lewis and Nocera, 2006*). On the downside, the price of current silicon-based solar panels is nearly seven-fold the cost of burning fossil fuels ($0.35 solar vs. $0.05 fossil per watt generated) (*Lewis and Nocera, 2006*). How to convert solar energy, a diffusive and discrete energy source, efficiently and inexpensively is one of the main focuses of today's research in chemistry.

Reported here is our initial effort to build molecular photovoltaic systems using lipid-based assembly strategies. Specifically, we present the assembly, characterization, and photocurrent generation of porphyrin/fullerene based photoelectrochemical system in aqueous media. As shown in Figure 1, this system can be assembled by first forming a self-assembled monolayer (SAM) on gold followed by a lipid monolayer created by liposome fusion, which gives a hybrid bilayer structure with porphyrin and fullerene directionally organized on the electrode. One important physiochemical parameter we studied here is the distance between photoactive fullerene and the underlying gold electrodes. According to the classical electron transfer theory, the electron transfer rate exponentially decays as the electron
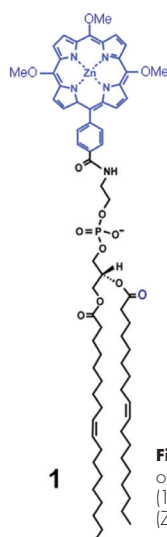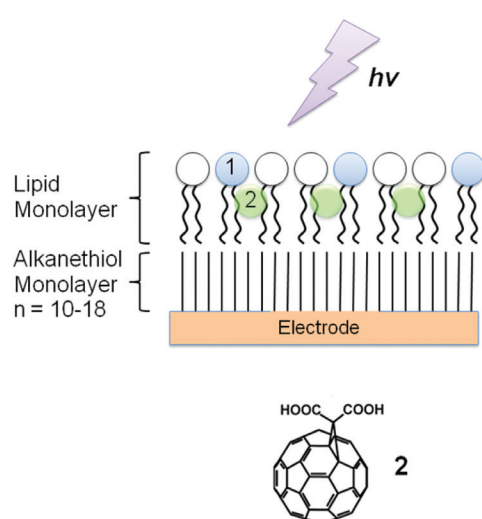
20

Figure 1. Experimental setup and species employed. Details of the device assembly can be found in the Experimental Section. (1) Zinc Porphyrin 1,2-Dioleoyl-sn-Glycero-3-Phosphoethanolamine (ZnP-DOPE). (2) C_{63} Fullerene.

transfer distance increases. On the other hand, short alkanethiols would yield less well-packed monolayers, which may adversely affect the deposition of the lipids on top of it. The fact that these two counteracting factors exist in the same system made us hypothesize that there might be a particular SAM on which a maximal photocurrent would be obtained. To this end, we have studied five *n*-alkanethiols containing 10 to 18 carbons.

Experimental Section

Reagents

Phospholipid 1-palmitoyl-2-oleoyl-*sn*-glycero-3-phosphocholine (POPC) was obtained from Avanti Polar Lipids. Alkanethiol agaents (C_nSH), 4-2-hydroxyethyl) piperazine-1-ethanesulfonic acid (HEPES), methyl viologen dichloride hydrate (MV^{2+}), L(+)-ascorbic acid sodium salt (sodium ascorbate), D-(+)-glucose, glucose oxidase (type X-S, from Aspergillus niger), and catalase from bovie liver were purchased from Sigma-Aldrich. All solutions employed in these experiments were prepared using 18.2 MΩ-cm deionized water (Millipore). Synthesis of monomalonic fullerene (C_{63}) (*Nitahara, et al., 2005*) and Zinc-porphyrin-conjugated 1,2-dipalmitoyl-*sn*-glycero-3-phosphoethanolamine (ZnP-DOPE) (*Zhan and Jiang, 2008*) was reported previously.

Assembly of Hybrid Bilayers

The preparation of hybrid bilayers has been reported previously (*Jiang et al., 2009*). The working area of the gold electrode used in these experiments was 1.13 cm². The gold substrates were formed by sputtering about 1,000nm of gold onto silicon wafers. The substrates were then cleaned with piranha solution (3:1 concentrated H_2SO_4/30% H_2O_2) for 15 minutes. The gold was then rinsed with H_2O, followed by ethanol, and then dried using Argon steam.

We followed a two-step process to form the photoelectrochemical cells. First, a self-assembled monolayer of alkanethiol was formed on a sputtered gold substrate. Next, liposomes of 1-palmitoy-1-2-oleoyl-1-*sn*-1-glycero-3-phosphocholine (POPC) incorporated with fullerene, porphyrin, or a combination of the two were prepared by extrusion. Exposure of the prepared liposome to the SAM completed the bilayer by immobilizing the photoactive agents in between the two lipid layers.

Photoelectrochemical Measurements

The ultraviolet-visible spectra (UV-Vis) were carried out using a UV-visible spectrophotometer (Cary 50 Bio, Varian). The fluorescence emission spectra of Zinc Porphyrin 1,2-Dioleoyl-sn-Glycero-3-Phosphoethanolamine (ZnP-DOPE) in liposome solutions were obtained using a Perkin-Elmer LS55 luminescence spectrophotometer. Standard 1-cm quartz cuvettes were used in both measurements.
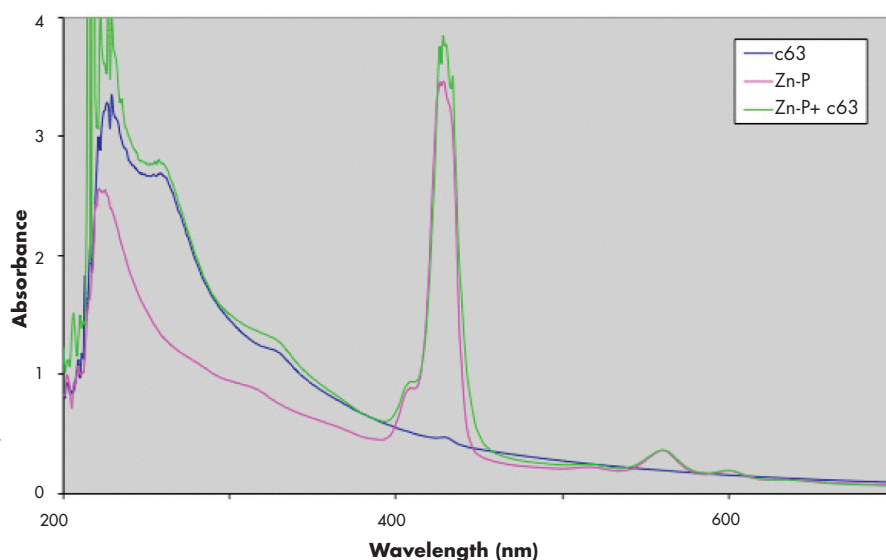
Figure 2. UV-visible spectra of liposome samples containing porphyrin, fullerene or their combination at 2 mol% in POPC.
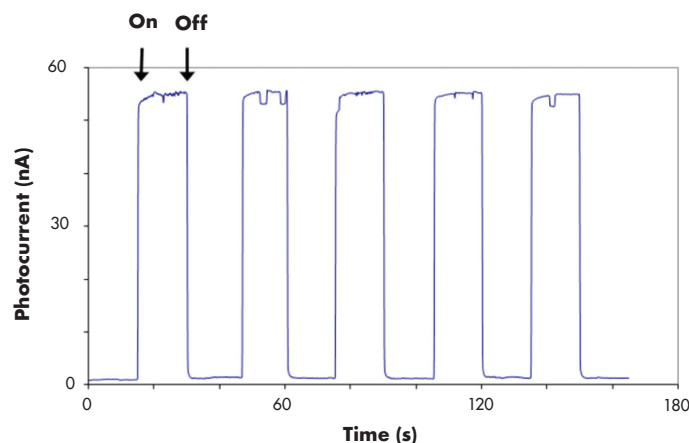
Figure 3. Typical photocurrents. This device contains 2% porphyrin deposited on a C8 alkanethiol SAM. Detailed photocurrent generation conditions can be found in the Experimental Section.

The electrochemical and photoelectrochemical measurements were carried out in a three-electrode Teflon photoelectrochemical cell. The three-electrode setup contains the gold (Au) substrate (with/without lipid SAMs or lipid bilayers) as the working electrode, Platinum (Pt), and Silver/Silver Chloride (Ag/AgCl) or (KCl saturated) as counter and reference electrode. The cyclic voltammetry experiments were conducted by a Personal Computer (PC)-controlled potentiostat (CHI 910B, CH Instruments) in 1.0 mM potassium hexacyanoferrate (III) in 1 M KCl and the scan rate was 100 mV/s. In the photoelectrochemical measurements, the electrolytes contain 50 or 100 mM NaCl in HEPES buffer. The cell was irradiated with light from a Mercury (Hg) lamp (X-Cite, Series 120 PC, EXFO) filtered at 417±30 nm (average intensity: 63.5 mW/cm²). Oxygen in the cell was removed by an enzymatic method used previously (*Nitahara et al., 2005*). This method utilizes a sacrificial electron donor that needs to be mixed 45 minutes prior to testing the anodic potential of each cell. This donor is a 1:1 mixture of ascorbate acid/GOX Enzyme (L(+)-ascorbic acid sodium salt, D-(+)-glucose oxidase).

Results and Discussion

System Design

As described in the Experimental Section, the photoactive porphyrin (**1**) and fullerene (**2**) are co-assembled in POPC liposome via an extrusion method. Subsequently, when they are deposited on the underlying alkanethiol SAM, the fullerenes are expected to be anchored in the hydrocarbon region of the phospholipids, whereas porphyrins reside directly at the top of the phospholipids near the water/lipid interface. As such, the two photoagents are organized on the electrode in a directional manner, with the fullerenes situated closer to the electrode. Since porphyrins are excellent electron donors for fullerenes under light excitation, an organized electron/donor pair will favor anodic photocurrent generation, in which case electrons flow from the solution towards the electrode.

Characterization of Devices

As shown in Figure 2, fullerenes and porphyrins can be readily incorporated into POPC liposomal hosts. Here, the main peaks at ~430 and 566 nm in the porphyrin sample can be assigned to electronic transitions from the ground state to the excited orbitals, S2 and S1, respectively; the absorption at 266 and 330 nm is associated with the strongly allowed transitions of fullerene C_{60}. Additionally, that the spectrum of the mixed sample ensembles the superposition of the individual ones indicates there is no significant electronic interaction between fullerene and porphyrin at the ground state.

A typical photocurrent response is shown in Figure 3. Here the excitation light is switched on and off every 15 seconds. Clearly, stable anodic photocurrent can be reliably obtained with this hybrid bilayer based photoelectrochemical cell.

Photocurrent Generation and Mechanisms

A primary concern within this report is the effect of varying SAM lengths on the obtained photocurrents. From previous studies as well as classical electron transfer theory (*Barbara et al., 2009*), we expect: 1) lower currents should be seen from devices comprised of longer alkanethiols; and 2) larger currents should be seen from devices containing porphyrin and fullerene co-assembled. Furthermore, the first prediction may be complicated by the fusion process of liposomes on a SAM, because a well-packed phospholipid monolayer can only be expected if the underlying SAM is smoothly packed as well (*Jiang et al., 2009*). As shown in Figure 4, for devices containing porphyrin only, the highest current is obtained when the underlying SAM is C14; for fullerene-only devices, a monotonic increase in photocurrents
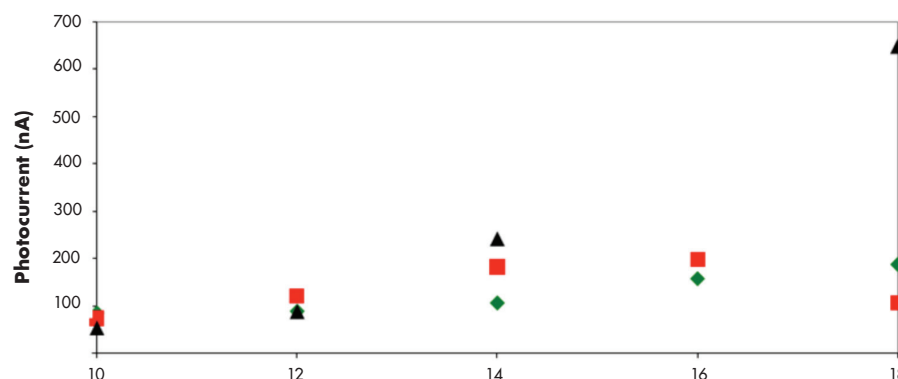
Figure 4. Comparison of photocurrents collected from 14 differently configured devices, containing 2% porphyrin (RED), fullerene (GREEN), or the two together (BLACK) on 5 alkanethiol SAMs.

is obtained as the SAM length increases from C10 to C18. This different trend between the two types of devices may be explained by the different deposition mechanisms associated with the two photoagents. For porphyrin, since it is directly tagged with a DOPE lipid, its deposition on the SAM should follow that of POPC, that is, a bilayer formation following hydrophobic/hydrophobic interaction between hydrocarbon regions of the two materials (*Plant, 1993*). By contract, since buckyball C_{63} are embedded in the lipid matrix instead of direct conjugation, a secondary, individual-specific buckyball/alkanethiol interaction mechanism might exist. Clarification of such a mechanism demands further investigations. Finally, for the devices comprised of the two immobilized together, we found again a monotonic increase as the SAM thickness increased. Although measurements of C16 based devices have not yet been performed, this trend is clearly shown by the other four devices. Higher currents from these two-component devices are expected because in these cases, both light harvesting and photoinduced electron transfer are accommodated.

Conclusions

The preliminary data described here demonstrate that different SAMs can indeed influence the obtained photocurrent in multicomponent, hybrid bilayer based, molecular photovoltaic systems. However, the trends observed cannot be simply explained by conventional rationales regarding electron transfer. These results may indicate that fullerenes can separate from their liposomal hosts and even form aggregations on the underlying SAMs, which, at least, explains the more-than-expected high photocurrents on longer SAMs. In the near future, we hope to address this issue by using other imaging techniques, such as atomic force microscopy (AFM).

References

Barbara, P. F., T. J. Meyer, and M. A. Ratner. (1996). Contemporary issues in electron transfer research. *Journal of Physical Chemistry*: 100 (31), 13148 – 13168.

Jiang, K., H. Xie, and W. Zhan. (2009). Photocurrent generation from ru(bpy)$_3^{2+}$ immobilized on phospholipid/alkanethiol hybrid bilayers. *Langmuir:* 25 (18), 11131.

Lewis, N. S. and D. G. Nocera. (2006). Powering the planet: Chemical challenges in solar energy utilization. *Proceedings of the National Academy of Sciences*: 103 (43), 15729-15735.

Nitahara, S.; T. Akiyama, S. Inoue, and S. A. Yamada. (2005). A photoelectronic switching device using a mixed self-assembled monolayer. *Journal of Physical Chemistry B:* 109 (9), 3944-3948.

Plant, A. L. (1993). Self-assembled phospholipid/alkanethiol biomimetic bilayers on gold. *Langmuir*: 9 (11), 2764-2767.

Zhan, W., and K. Jiang. (2008). A Modular Photocurrent Generation System Based on Phospholipid-Assembled Fullerenes. *Langmuir:* 24 (23), 13258-13261.

Zhan, W., K. Jiang, K. D. Smith, M. L. Auad, J. V. Ruppel, C. Kim, X. P. Zhang, and M. D. Best. (2010). Photocurrent Generation from Porphyrin/Fullerene Complexes Assembled in a Tethered Lipid Bilayer. *Langmuir*: 26 (19), 15671-15679.

The Effectiveness of Systematic Subsurface Testing on a Multicomponent Site in Northern Macon County, Alabama

Hamilton H. Bryant III and John W. Cottier

ABSTRACT

From 1997 until 2011, field investigations were conducted at the archaeological site 1Mc25, a multicomponent Woodland and Mississippian cultural resource located in central Alabama. Investigations in 1997 and also in 2010 included the use of auger testing over significant portions of the site as a data recovery method. Subsequent research at 1Mc25 used data generated from auger testing and geophysical remote sensing techniques to evaluate the effectiveness of these testing techniques for assessing the distribution of specific artifact forms, identifying the intensity of human utilization of selected areas within the site, and guiding the placement of more substantial excavation units. This paper summarizes the results of the testing methods and examines their utility.

INTRODUCTION

In archaeological studies it is often impossible to reliably locate subsurface features and deposits through surface inspection alone. This difficulty can result from many years of vegetation growth, natural geologic deposition, farming activities and other elements. These factors are common in the United States east of the Mississippi River, and constitute one reason for the use of remote sensing or subsurface testing techniques. Subsurface testing, typically accomplished through shovel testing, refers to techniques that physically recover material remains from beneath the surface. In areas of the western and southwestern United States, where there is little deposition or vegetation covering the ground, sites may be identified by visual inspection alone. In a systematic subsurface investigation, small-scale excavations may be hand-dug or machine augered at specific points along a grid at regular intervals.

Over the thousands of years that humans inhabited the United States many locations were equally desirable for various peoples at different periods. An attractive location may have been inhabited by a band of nomadic hunter-gatherers 3,000 years before a sedentary village of agricultural dwellers from the Mississippian cultural period (700 A.D. – 1500 A.D.) farmed the land. As a result there are artifacts and features that span the entire period of the site's occupation. The types of artifacts present at a site change over time and may be diagnostic of specific time periods. The physical form of artifacts also changes over time (e.g., the evolution of Coca-Cola containers). At the Ebert Canebrake site (1Mc25), in Macon County, Alabama, occupations from the Archaic, Woodland and Mississippian cultural periods have been identified, making it a complex, *multicomponent* site (Table 1).

Assigning any one feature to a particular period may be possible if there are associated diagnostic artifacts or the recovery of

Table 1. Regional Cultural Chronology (Walthall, 1980).

HISTORIC A.D. 1700-Present
PROTO-HISTORIC A.D. 1500-A.D. 1700
MISSISSIPPIAN A.D. 700-A.D. 1500
WOODLAND 1,000 B.C.-700 A.D.
ARCHAIC 8,000 B.C.-1,000 B.C.
PALEO-INDIAN 10,000 B.C.-8,000 B.C.

remains that are datable through methods such as Carbon-14 analysis. However, collecting these artifacts often requires actual excavation. Subsurface investigation of a site may be accomplished through subsurface testing such as using an auger to dig small, regular holes or through remote sensing methods, which are often preferred due to their non-destructive nature.

Despite the multicomponent nature of the site, research at Ebert Canebrake has focused on the small but significantly fortified Mississippian village. Subsurface testing, in conjunction with a variety of geophysical remote sensing techniques, was undertaken to provide a better understanding of component-specific cultural behavior, such as fortification construction and purpose, at Canebrake. In this study, we use artifact data recovered through auger testing in 1997 and 2010 and information provided by geophysical remote sensing to explore the cultural aspects of this multicomponent site. The data generated from the auger testing were tabulated and entered into a Geographic Information System (GIS) in 2011. With the help of the GIS, we were able to construct artifact-specific contour maps that demonstrate patterns of clustering and vacant areas. These data compared with the magnetic data provide an opportunity to study the effectiveness of magnetic gradiometry for locating cultural features at this important prehistoric site. Through the analysis of culture specific artifacts (such as diagnostic ceramic types and daub, a type of baked clay) we hope to have a better understanding of systemic cultural behavior over time at Ebert Canebrake.

BACKGROUND

The Ebert Canebrake site was first identified in the early 1960s. At that time, the site was intermittently cultivated, with limited surface visibility. In 1978, Auburn University purchased the property, which included over 3,816 acres within the Tallapoosa River alluvial valley and contains the Ebert Canebrake site, from the Walker family for use as an agricultural research center (*Cottier and Sheldon, 1999*). The Ebert Canebrake site is now considered a protected portion of the E.V. Smith Research Center. Over the last decade archaeological research has focused on revealing more about the nature of Woodland and Mississippian occupations at the site. This research has included a variety of traditional archaeological testing regimens, as well as more advanced geophysical prospection.

The site is located along the south bank of the Tallapoosa River at the mouth of Calebee Creek (Figure 1). The archaeological remains are concentrated along a clearly defined river levee at an elevation of 180 to 190 feet above mean sea level (*Cottier and Sheldon, 1999*). The site is located south of an abrupt increase in elevation associated with the Fall Line Hills, and north of the Black Belt Prairie, a subdivision of the East Gulf Coastal Plain physiographic region (*Mason, 1998*). The Fall Line Hills are composed mainly of Piedmont crystalline rocks, while the Black Prairie is associated with the Late Cretaceous sedimentary rocks of the Eutaw Formation (*Mason, 1998*). The Tallapoosa River alluvial valley is dominated by extinct stream channels, including oxbow lakes and cypress swamps, small- and medium-sized streams, and numerous small and low ridges of fertile and friable soils typically found throughout the lower Tallapoosa River Valley (*Cottier and Sheldon, 1999*).

Previous research at the site has established that Ebert Canebrake was intermittently occupied from the early Archaic through the late Mississippian (*Cottier and Sheldon, 1999*). Fontana (2007) has suggested that the Mississippian occupations began during the Shine II Phase, circa A. D. 1350, and continued through the Moundville-related Big Eddy Phase, circa A. D. 1450. Currently, several Woodland occupations, the Mississippian occupation, and a limited Historic Creek occupation have been identified. After more than a decade of archaeological research at Ebert Canebrake, our attention remains fixed on the nature and chronology of the Mississippian fortification system. The following section discusses our methods and procedures for the years pertinent to a comparison of our auger testing, subsequent ground truthing, and geophysical remote sensing work.
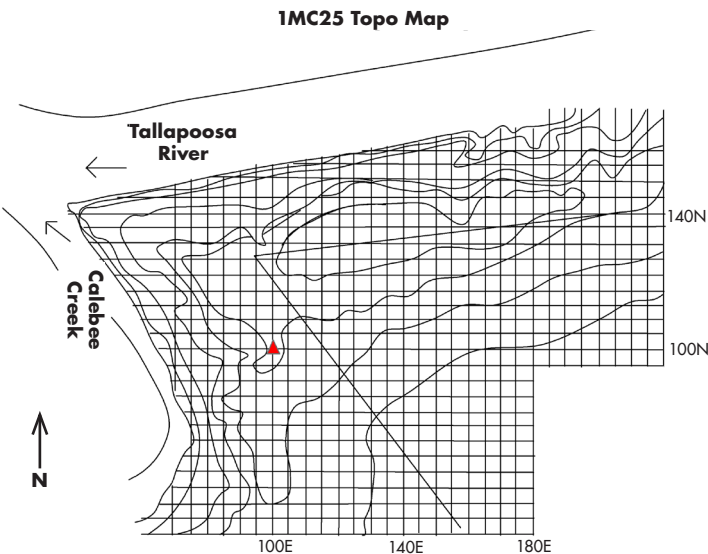
25

Figure 1. Topographic map of the Ebert Canebrake Site. The scale is in meters. Visible features include Calebee Creek, Tallapoosa River, site benchmark and fence that surrounds the pasture portion of the site.

METHODS AND PROCEDURES

During the summer of 1997, the Auburn University archaeology program conducted a field program within the E. V. Smith Research Center. Attention was directed to several archaeological resources including the Ebert Canebrake site. A visit to the site identified a recent looters' pit near the bank of Calebee Creek. Material from this pit was screened, revealing a large collection of Mississippian ceramics. At that time, the site was mapped and a grid established. Additionally, it was decided to test the site using a tractor-mounted auger (*Oggs, 2003*). Tests were approximately 30 cm in diameter and made at 5 m intervals along the site grid. This testing was expected to help delineate site boundaries, provide stratigraphic information and demonstrate possible cultural affiliations. The standard procedure included first clearing a 50 cm by 50 cm area with a flathead shovel. The auger was then used to drill a hole to an average depth of approximately 60 cm below surface. Excavated soils were then removed using a posthole digger and hand scoops, and source locations were marked. Recovered soils were then screened through a ¼-in mesh. Profiles were not drawn but notes were taken on the presence, depth and unusual characteristics of soil stratigraphy, with the purpose of identifying the distribution of the Mississippian strata and any potentially valuable anomalies. Like the process employed at Moundville by Steponaitis (*2009*), we discovered the most efficient method was to split into teams. One team cleared the grass and dug the holes while several other teams followed the tractor sifting the soil, refilling the holes, taking notes and bagging the artifacts. This process was repeated over a two-month period.

The 1997 investigation produced a wide variety of artifacts, including an unexpectedly large sample of fired daub. Artifacts were tabulated and weighed in a laboratory established on site. Based on this analysis, two small trenches were opened in areas with the highest concentrations of daub. Both trenches encountered thick middens with concentrations of shell tempered ceramics and extensive architectural daub beneath a shallow plow and alluvium level. The shallow surface zone was referred to as Zone A, the Mississippian strata as Zone B, and a mixed Woodland and Mississippian level as Zone C.

The site was revisited in 1998 as part of the Expedition Program of the Museum of Natural History at the University of Alabama. At this time, two separate investigations were conducted; one was a 1 m by 16 m trench along the 91 east line and the other a larger excavation unit approximate 4 m by 10 m (Figure 1). The location of this unit was based on the high occurrence of daub identified in the 1997 testing program. This excavation demonstrated the occurrence of three separate, superimposed domestic structures with puddled clay floors, prepared clay hearths, postholes, and extensive fired daub and shell-tempered ceramics. The trench along the 91 east line demonstrated evidence of a possible fortification system along both the creek and river sides.

The field season in 1999 continued to place an emphasis on identification of the possible fortification system through the excavation of several short trenches that attempted to intersect its projected path (lines 81E, 86E and 100E). The 86E trench revealed significant quantities of architectural daub as well as debris associated with domestic activities (e.g., ash, charcoal, nuts) suggesting possible fill associated with the fortification ditch. The 81E trench produced no evidence of the fortification while the 100E trench produced daub concentrations and postholes, suggesting a possible palisade. Many diagnostic potsherds were recovered during the excavation of these trenches. These sherds exhibited an assortment of stylistic treatments ranging from intricate incising and stamping to rim effigies (*Oggs, 2003*). At the end of this summer field season, the 86E trench had produced the most conclusive evidence of the fortification system.

During the 2002 field season, a ground-penetrating radar (GPR) survey was made of a select portion of the site. As Hargrave (*2011*) has noted, one common trait of complex prehistoric archaeological sites that can reduce the utility of GPR surveys is the presence of a clay-rich midden, like that which occurs at the Ebert Canebrake site. Unfortunately, this characteristic led to poor results from the GPR survey because highly conductive concentrations of daub produced signal distortion (*Fontana, 2007*). Basic excavation of units, opened where they ended the previous summer, were extended eastward in an attempt to expose larger portions of previously uncovered palisade sections. By mid-June a sand wash clearly associated with the fortification

had been identified at 115N/92E (*Oggs, 2003*). Excavations east of the 86E trench demonstrated another puddled clay floor associated with a domestic structure not the fortification. Carbon samples were taken; however, none from dateable charred palisade posts were recovered. The resulting dates place the Mississippian occupation of Canebrake into two main periods between the mid-1300s and the mid-1400s (*Fontana, 2007*).

In 2009 select portions of Canebrake were explored by a joint field school, in which a magnetic gradiometer was used. The goal of this exercise was to familiarize students with the use of a gradiometer and to better define possible intact subsurface features, such as houses and the fortification system. Gradiometry has been useful in locating walls and trenches in numerous similar settings (*Bigman et al., 2011; Kvamme and Ahler, 2007*). The survey was conducted using standard magnetic survey methods. Magnetic data were collected using a single-pole Bartington 601 fluxgate gradiometer in a series of 10 m by 10 m units at a 1 m traverse interval and 0.25 m sample interval (four readings per meter). The traverses transcended the 10 m by 10 m units at the edge of the fence line, bordering the creek and riverside of the creek, and continued to the central portion of the site. It was necessary to maintain a 5 m distance from the fence to minimize magnetic interference. As a result, the northern and western borders of the site were not investigated using this procedure because of their proximity to the fence. The corners of each 10 m by 10 m unit were established using a total instrument station. Tape measures were used to ensure that each surveyor maintained a constant pace and to guide data collection. Magnetic data were processed to remove extraneous readings and analyzed using ArchaeoSurveyor™ 2.5.

The geophysical data collected identified numerous anomalies (Figure 2). The highest concentration of anomalies was present in the western portions of the survey area, and a significant absence of magnetic anomalies was observed in a pattern from the southwestern area of the site moving east and then north. The areas with the least complex magnetic signals are thought to correspond with areas outside the previously identified fortification system. Time constraints and the educational nature of the investigations limited our survey to an irregular area.

The 10 m by10 m unit in the northeast corner of the survey area contained the highest density of magnetic anomalies. In general, the riverside axis of the site has been found to have higher concentrations of Woodland cultural remains, so these anomalies may be related to the Woodland Period occupation of the site. The distribution of shell-tempered ceramics from auger testing also supports this interpretation, as few shell-tempered ceramics were recovered from this area.

During the winter of 2009 additional remote sensing was conducted with students from the Department of Geology and Geography at Auburn University. It was hoped that the results of an additional, complementary geophysical technique could be compared with the results of auger testing and previous remote sensing (*Clay, 2001*). The investigation used a 48-electrode Advanced Geoscience Inc. (AGI) SuperSting™ resistivity meter for 3D electrical resistivity tomography (ERT). The data were inverted using AGI's EarthImager™ software to obtain a realistic subsurface distribution of ground conductivity. The 14 m by 20 m grid was designed to partially coincide with one of the areas of interest identified by the gradiometer survey. The recovered data showed a large continuous anomaly beneath the plow zone. However, whether this feature was cultural or geological could not be

determined from the ERT data.

During the summer of 2010 the Auburn archaeology program initiated another auger testing survey to investigate the remaining portions of Canebrake, as well as numerous other locations within the E. V. Smith Beef Cattle Unit. This was in part motivated by the results of the magnetometry survey in 2009. The procedure was almost identical to that employed in 1997; however, the results were much less remarkable. The testing began at the 200E line and the interval ranged from 5 m to 20 m, depending on magnetic anomalies detected by the gradiometer. This testing did little to further knowledge of artifact distributions or the extent of the Mississippian settlement area.

ANALYSIS AND RESULTS

To understand component-specific, subsurface features and artifact distribution at Ebert Canebrake, we analyzed the artifacts recovered from auger testing and compared results with the geophysical data. The first step of the data analysis involved classifying artifacts into meaningful categories. One methodological concern was establishing contemporaneity of the remains in any given pattern. This is not a new problem in archaeology, but of importance especially in a multicomponent site. Certain categories of artifacts are easily distinguished

by component, whereas others (such as cracked rock) are not as readily sortable.

Once categories were established and artifacts measured (either counted or weighed) the information was organized by the site grid format to create a computer database for the auger testing. The datasets were interpolated using ArcGIS to provide distributional levels, and these levels displayed on the grid format. This approach is a simple means of displaying and analyzing distributions of artifact groupings, but does not in itself explain any of the actual distributions. In the specific cases utilized for this paper, displays have been prepared for artifact groupings most relevant to the Mississippian and Woodland period occupations (Figures 3, 4 and 5). These illustrate several patterns that are potentially informative.

Results of the auger testing at Canebrake yielded recognizable patterns in the distribution of specific artifact forms recovered. The artifact forms reported here are Mississippian daub, and shell-tempered and sand-tempered ceramics. In general, the distribution of concentrated quantities of all artifacts decreases from west to east. Of particular interest is the impressive amount of daub recovered in the 1997 auger testing that ended at approximately the 200E line (Figure 3). The 2010 testing, beginning at the 210E line, recovered drastically less daub, in terms of weight, although the testing interval was larger in most cases. We interpret this to indicate tests inside and outside, respectively, of the domestic settlement and the fortification system. This provides a significant result in terms of locating the western boundary of the fortification system and the Mississippian occupation of the site. Likewise, we have interpreted the lack of shell-tempered Mississippian sherds recovered east of the 200E line to reflect a similar pattern (Figure 4), indicating that auger tests were located inside and outside of the fortification. What might seem surprising is that the distribution of sand-tempered Woodland ceramics reflects a similar pattern, if to a lesser degree (Figure 5). We attribute this similarity to topography. As previously stated, the highest concentration of Woodland cultural material is found along the elevated levee running parallel to the river and the creek. Around the 200E line, the surface elevation slopes to the south and east, if only slightly. Additionally, more sand-tempered ceramics were recovered
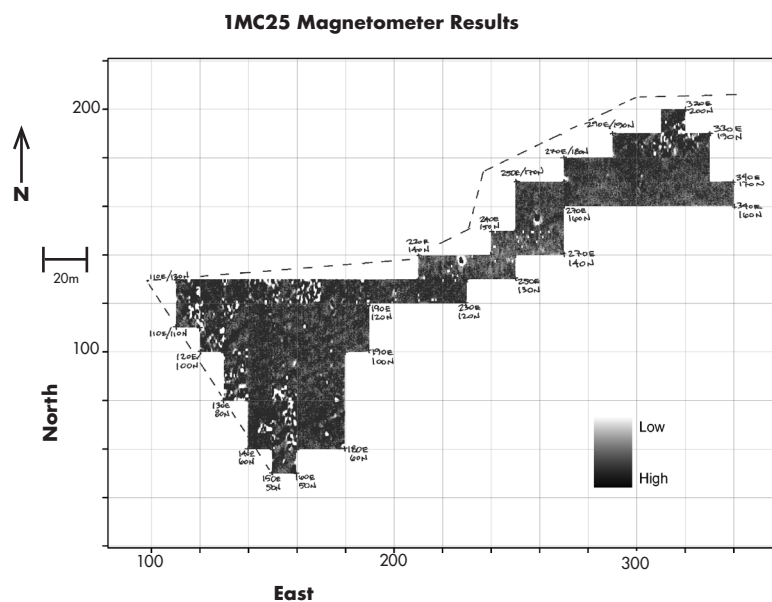
Figure 2. Illustration of magnetometry data overlain on the site grid. Dashed line represents fence line separating pasture (interior) portion of site from wooded portion. Dark colors represent high magnetic readings and light colors represent low magnetic readings.
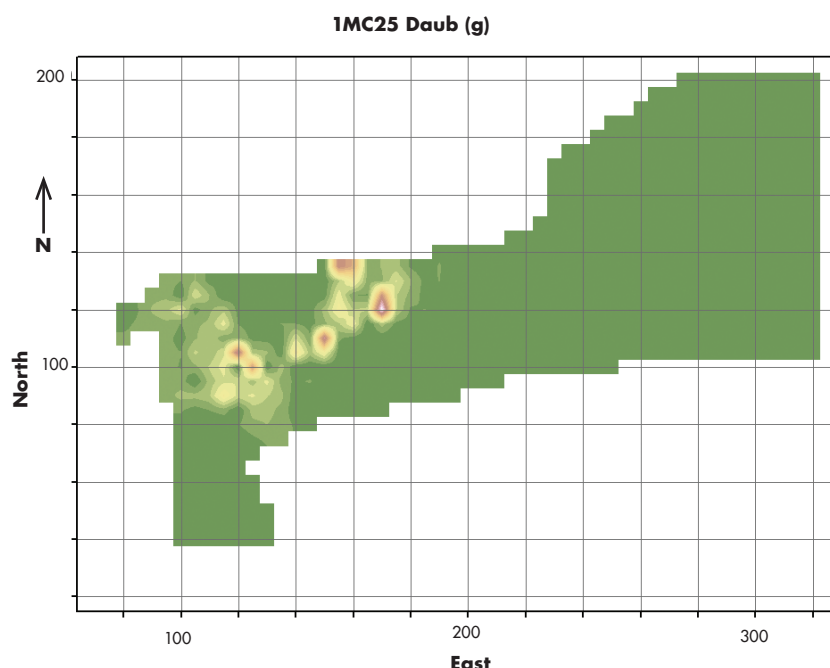
1MC25 Daub (g)

Figure 3. Distribution of fired daub recovered during auger testing in 1997 and 2010. Warm colors indicate higher density of daub recovered. Note open space within the ring of high density daub.
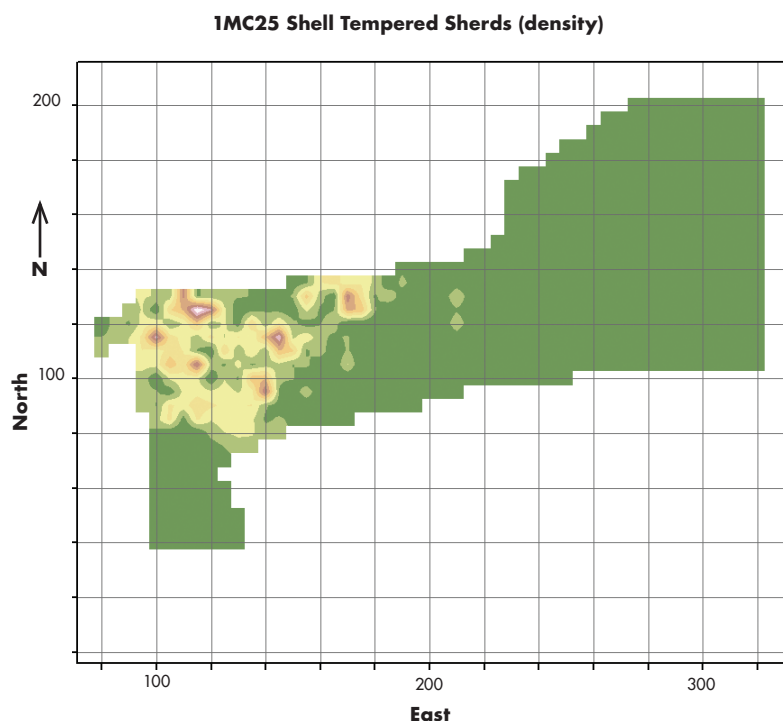
1MC25 Shell Tempered Sherds (density)

Figure 4. Distribution of shell-tempered (Mississippian) ceramic sherds recovered during auger testing in 1997 and 2010. Warm colors indicate higher density of sherds. Note the highest density in northwestern corner of survey area.

in the northern and northeastern survey area, which is located on the more elevated portions to the north of the low area. In other words, the occurrence of higher concentrations of shell-tempered and sand-tempered ceramics within the area bounded by the projected Mississippian fortification reflects the fact that the higher elevated areas of the site were desirable to people of Woodland and Mississippian groups, rather than contemporaneous sand and shell tempering peoples. An alternative suggestion might be that this pattern is illustrative of site formation processes (i.e., post-depositional, taphonomic disturbances), or what Schiffer (*1975*) has termed N-Transforms, or natural transformations. Undoubtedly, Canebrake is not completely level; however, the hydrologic forces at work and the slight slope at the site are not significant enough to create the observed pattern. Furthermore, if river action were responsible for the patterns observed, then the concentrations would occur in the low areas of the site, not the areas of higher elevation. It should also be noted that in the areas of the highest concentration of auger tests were the areas of the highest percentages of artifacts. To some degree, this reflects inconsistencies in the sampling strategy.

The daub distribution reveals a potentially important pattern of open space surrounded by extensive daub concentrations (Figure 3). This may represent a portion of the site associated with different systemic behavioral patterns than that represented by the surrounding zone. Such an enclosed central location could potentially delineate some form of public space, such as a square ground. This type of feature, if verified, would represent a significant difference in the spatial and social organization between the Woodland and Mississippian period occupations of Ebert Canebrake. However, the presence of such a public space, or square ground, may not be proven without extensive, and damaging, excavation. The distribution of shell-tempered sherds demonstrates a similar pattern, but it is less distinct.

To compare the magnetic data with the artifact distributions recovered by the auger survey, we made a basic visual comparison of the distribution images with

the magnetic data. In ArcGIS we overlaid a transparent image of the artifact totals on top of the magnetic data. This allowed us to make more nuanced observations concerning the agreement between our data sets. Due to the complex nature of the image, we have not reprinted it here. As expected, we observed that our methods produced comparable results in locating subsurface features. With that said, augering and geophysical remote sensing each have advantages and disadvantages. Augering is slower and more labor intensive but, as Steponaitis (*2009*) reported, it has the advantage of producing artifacts and profiles of soil stratigraphy. Also, power augering has the benefit of not being heavily reliant on weather conditions or proximity to metallic material such as fence wire. Despite the sometimes paltry quantities of artifacts recovered per auger test, we were able to get a preliminary sense of when each area was occupied. However, this method of augering is relatively damaging to the archaeological record.

Geophysical exploration is known to provide complementary data to auger testing and other excavation methods (*Clay, 2001; Gaffney and Gater, 2003; Steponaitis et al., 2009*). Geophysical prospection at Canebrake has the advantage of providing more continuous data that can readily identify large and small subsurface features that are easily missed by the fragmented picture provided by the auger holes. The ability of remote sensing to check and balance standard archaeological testing techniques is one of the many reasons to employ multiple methods of subsurface exploration at complex archaeological sites.

CONCLUSIONS

The spatial distribution of artifacts at the Ebert Canebrake site contributes to an understanding of the site as a human settlement. The auger testing performed in 1997 and again in 2010 has by far been the most illuminating procedure in terms of demonstrating site size and specific occupational clusters. The additional geophysical methods used at the site helped to identify areas for closer examination in future studies. Results of the study suggest that the site was most heavily occupied on the elevated areas by each of the various
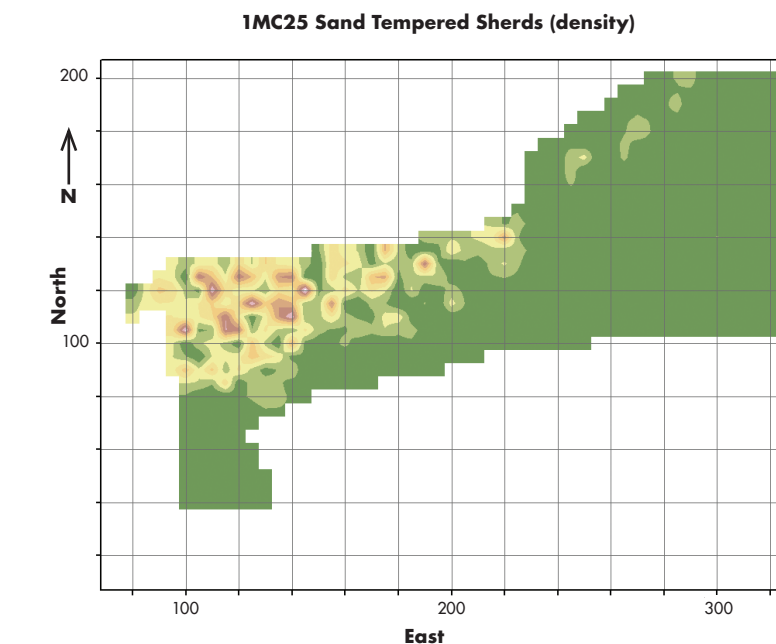

1MC25 Sand Tempered Sherds (density)

Figure 5. Distribution of sand-tempered (Woodland) ceramic sherds recovered during auger testing in 1997 and 2010. Warm colors indicate higher density of sherds. Note the highest density in northwest corner of survey area.

peoples occupying Canebrake. The presence of a possible public square ground illustrates a significant contrast between the spatial organization and community planning of the Mississippian and Woodland period occupants of Canebrake. Public spaces, such as a plaza or square ground, are not simply vacant space that developed because architecture enclosed an open area; they must be understood as one of the central design elements of intrasite spatial organization. Without extensive excavations this interpretation is difficult to prove or disprove. The use of geophysical remote sensing and auger testing provided complementary data, which has given us a better understanding of the size, distribution and chronological position of archaeological deposits at Canebrake. These data will be used to precisely guide future excavations and avoid unnecessary damage to this important archaeological site. Our investigations will continue to explore the internal distributions and relationships of artifacts and features in both the excavated and unexcavated portions of the site. Hopefully, such study will elucidate in part the spatial organization of this important multicomponent site in central Alabama.

REFERENCES:

Bigman, D. P., A. King and C. P. Walker (2011). Recent geophysical investigations and new interpretations of Etowah's Palisade. *Southeastern Archaeology*: 30(1), 38-50.

Clay, B. R. (2001). Complementary geophysical survey techniques: Why two ways are always better than one. *Southeastern Archaeology*: 20 (1), 31-43.

Cottier, J. W. and C. Sheldon. (1999). Archaeological investigations at the Ebert Canebrake site, central Alabama. Unpublished Manuscript, Auburn University Archaeology Lab, Auburn, Alabama, United States.

Fontana, M. D. (2003). Quandaries at Canebrake: Excavation at 1MC25. Unpublished Manuscript, Auburn University Archaeology Lab, Auburn, Alabama, United States.

Fontana, M. D. (2007). Of walls and war: Fortification and warfare in the Mississippian southeast. Ph. D. dissertation. Department of Anthropology, Chicago, Illinois: University of Illinois at Chicago.

Gaffney, C. and J. Gater. (2003). *Revealing the Buried Past, Geophysics for Archaeologists*. Gloucestershire: Tempus.

Hargrave, M. L. (2011). Geophysical survey of complex deposits at Ramey Field, Cahokia. *Southeastern Archaeology*: 30(1), 1-19.

Kvamme, K. L. and S. A. Ahler (2007). Integrated remote sensing and excavation at Double Ditch State Historic Site, North Dakota. *American Antiquity*: 72(3), 539-561.

Mason, J. M. (1998). *Soil Survey of Macon County, Alabama*. Washington: U.S. Department of Agriculture.

Oggs, R. D. (2003). Postulations on Mississippian warfare: Examination of the defensive works at Ebert Canebrake: 1Mc25, M.A. thesis. Department of Sociology, Anthropology and Social Work, Auburn, Alabama: Auburn University.

Schiffer, M. W. (1975). Archaeology as behavioral science. *American Anthropologist*: 77 (4), 836-838.

Steponaitis, V. P., R. P. S. Davis and H. T. Ward. (2009). Field evaluation of two subsurface augering methods at Moundville. *Southeastern Archaeology*: 28(2), 259-267.

Walthall, J. A. (1980). *Prehistoric Indians of the Southeast: Archaeology of Alabama and the Middle South*. Tuscaloosa: University of Alabama Press.
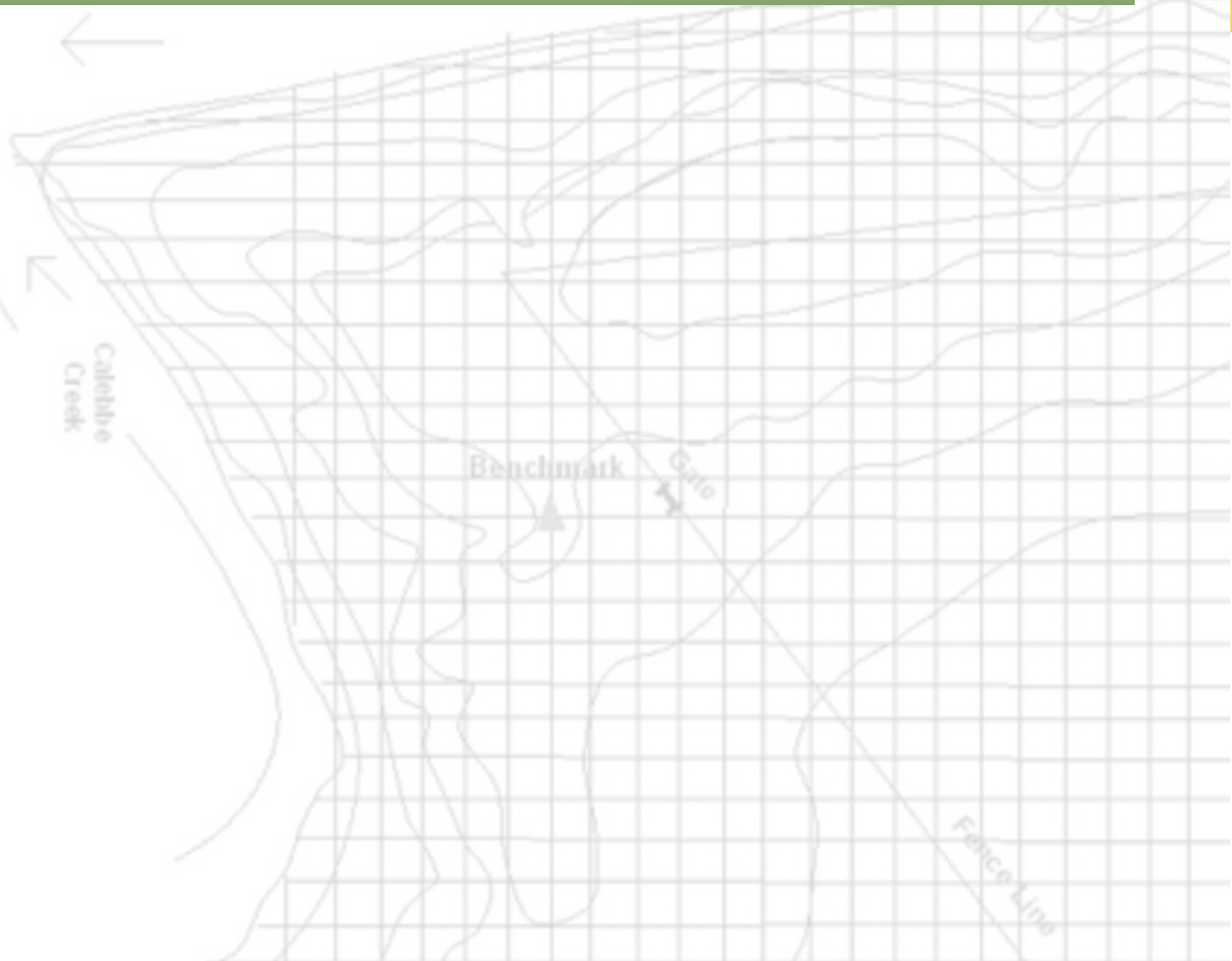
Carbon and Nitrogen in Soils Under Differing Cotton Rotations in Auburn University's Historic Old Rotation Experiment

Leffie V. Dailey, C. Wesley Wood, Brenda H. Wood, Charles C. Mitchell

Abstract

Crop rotations influence carbon and nitrogen amounts in the soil, and therefore have an impact on soil carbon sequestration and nitrogen availability for plant growth. The objective of this experiment was to determine soil carbon and nitrogen concentrations under various crop rotations of the *Old Rotation* located on the campus of Auburn University. Soil samples (0 to 5 cm) were taken from each of the 13 long-term (>100 years) cotton rotations. A composite sample was made for each of the 13 plots by combining 10 random samples. The two plots with the lowest amounts of carbon and nitrogen were those with no cover crop or added nitrogen, and the plot with the most carbon and nitrogen was planted on a three-year rotation of cotton, legume cover, corn, grain, and soybean. Based on this experiment it is important to manage crop rotations to maintain soil quality.

Introduction

Since 1750, carbon dioxide (CO_2) concentrations in the atmosphere have increased due to consumption of fossil fuels by combustion and land-use change. Carbon emissions due to land use originate from deforestation, burning of biomass, creation of agricultural systems, destruction of wetlands, and soil cultivation. These practices have significantly increased atmospheric CO_2, which is said to cause global warming *(Lal, 2004)*.

Unlike carbon, which is stored in bulk in soils, the majority of the Earth's nitrogen is stored in igneous rocks located in the mantle and is unavailable to plants. Atmospheric nitrogen (N_2) is the origin of nitrogen used by plants, but it has to be "fixed," either by rhizobacteria in association with legumes, or industrially in fertilizer factories. Most nitrogen in the soil is in organic forms, which must be mineralized to inorganic forms before plants can use it. Most cotton growers use fertilizer nitrogen to meet cotton needs, but nitrogen fixed by legumes in rotation with cotton could supply much of cotton's nitrogen needs as the "green manure" decomposes and releases nitrogen. Nitrogen from legumes not immediately mineralized adds to organic nitrogen storage and improves soil quality.

The *Old Rotation* is located on the campus of Auburn University. It was established in 1896 and has been used continuously for cotton production for over 115 years *(Mitchell et al., 2008)*. The *Old Rotation* is the oldest

continuous cotton study in the world *(Mitchell et al., 2008)*. The purpose of the *Old Rotation* is to exhibit and study the effects of crop rotation and fertilization on cotton production. The site has been used for educational and scientific purposes throughout the years, including in soil-quality studies. The *Old Rotation* contains 13 treatment plots that represent continuous cotton, or cotton grown in rotation with other crops (Table 1). The purpose of this experiment was to determine the impact of long-term cotton crop rotation on surface soil carbon and nitrogen concentrations.

Materials and Methods

Soil samples (0 to 5 cm depth) were collected on August 30, 2011, from the *Old Rotation* site. Ten cores were combined to make one composite sample from each plot for analysis. The 13 different composite samples were dried for one week at 60°C in a drying oven. After drying, each sample was sifted to pass a sieve with 2 mm openings, and a small portion of each sample was finely ground using a mortar and pestle to produce the final sample for analysis. The finely ground samples were weighed to approximately 0.2 g, and analyzed via combustion with a LECO Truespec CN Autoanalyzer (LECO Corporation, St. Joseph, Minnesota). Samples from each treatment plot were run in triplicate.

Results

Table 2 shows the total carbon and nitrogen in the soil samples from plots 1 through 13 in the *Old Rotation*. The

plots containing the highest amounts of carbon were plots planted with a legume cover crop (Tables 1 and 2). The plots that had no legume cover crop not only had the lowest amount of sequestered carbon within the upper 5 cm, but the carbon concentrations were approximately one third less than that of plot 11, which contained the highest amount of carbon sequestered for all 13 plots.

The plots containing the most nitrogen were those having a nitrogen-fixing legume cover crop as part of the cotton rotation. Both plot 8 and plot 11 had a legume cover crop

Table 2. Total carbon and nitrogen concentrations in soil samples (0 to 5 cm depth) from 13 plots at Old Rotation study area, Auburn University, Alabama

Plot number	Carbon (g/kg)	Nitrogen (g/kg)
1	8.2	0.58
2	19.5	1.18
3	17.9	1.10
4	21.7	1.28
5	26.5	1.56
6	7.1	0.54
7	15.4	1.01
8	27.1	1.54
9	23.5	1.42
10	21.1	1.23
11	28.2	1.56
12	21.4	1.28
13	17.8	1.06

Table 1. Crop rotation configurations and fertilizer applications for plots at the *Old Rotation*. CC = continuous cotton; w/o cover = no cover crop; FB = followed by

| Plot Number	Crop Rotation	Fertilizer application rates (pounds per acre of nitrogen/year)
1 and 6	CC w/o cover	no nitrogen applied
2, 3, and 8	CC with legume cover	no nitrogen applied
4 and 7	two-year rotation of cotton - corn and legume cover	no nitrogen applied
5 and 9	two-year rotation of cotton - corn and legume cover	120 lbs on cotton and corn, no nitrogen added for winter legume
10, 11, and 12	three-year roation of cotton FB a legume cover crop FB corn FB wheat or rye (as a grain) FB soybean	only 60 lbs on wheat or rye, 0 applied for cotton, corn, soybean, and winter legume
13	CC w/o cover	120 lbs
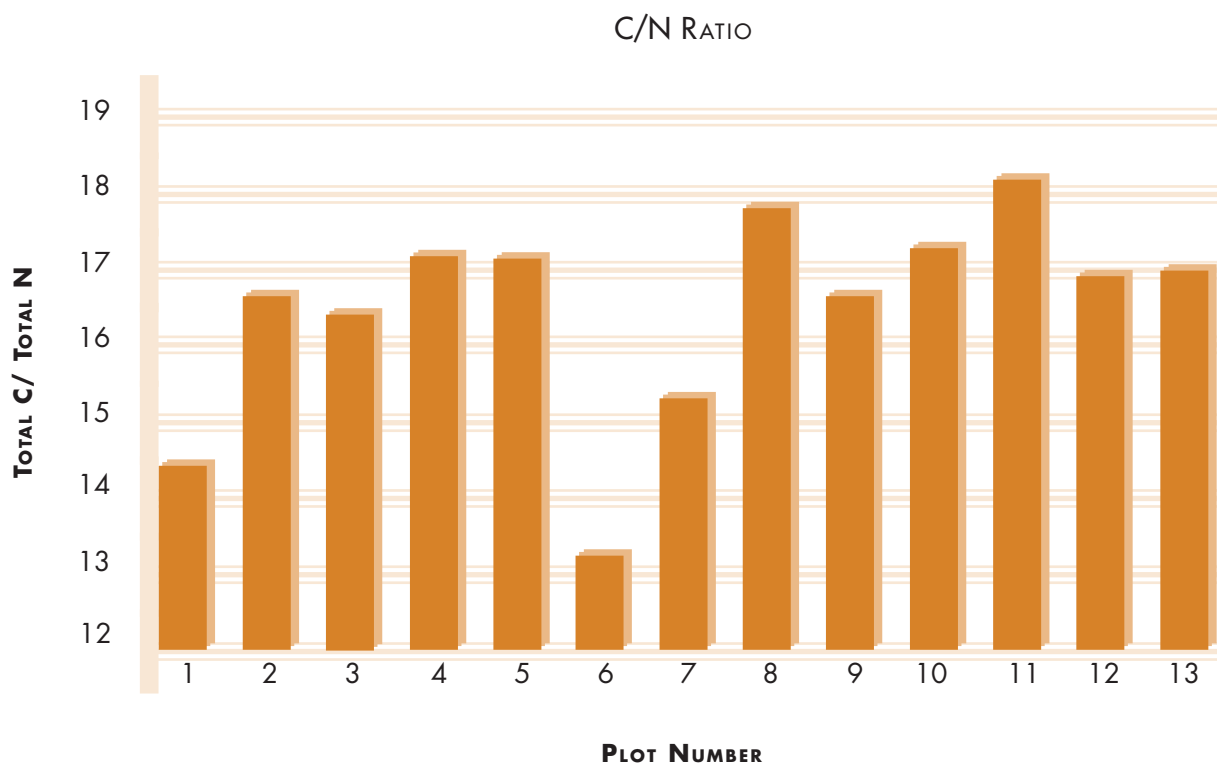
C/N Ratio

Figure 1. C/N ratio by plot number at Old Rotation, Auburn University, Alabama.

(Table 1). However, plot 11, with the highest amount of nitrogen in surface soil, was planted on a three-year rotation of cotton followed by the legume cover crop, corn, a grain, and soybeans (Table 1). As expected, the plots with the lowest amounts of nitrogen in the soil were those plots that are not planted with a cover crop of any type, which resulted in roughly one third less than that found in plots with a legume cover crop (Table 2). These data show that rotations containing nitrogen-fixing legumes provide more nitrogen in surface soils than that of the rotations without a nitrogen-fixing cover crop.

Discussion

The largest terrestrial pool of carbon is contained in soils. Physical properties of soils can be enhanced by carbon. For example, soil cation-exchange capacity, soil water-holding capacity, and soil aggregation are all improved with increased concentrations of soil organic carbon *(Leeper, 1993)*. Organic matter in the soil plays a large role in plant growth by holding nutrients, cations, and other

trace elements that are needed in order for plants to be productive *(Leeper, 1993)*. Drinkwater (2003) notes that carbon and nitrogen cycling through organic matter can improve soil fertility and yields, and reduce the environ-mental effects of CO_2. Our study indicates that including legume cover crops in rotation with cotton results in greater soil carbon sequestration, which in turn provides a higher quality substrate for crop plant production. Moreover, greater soil carbon storage owing to inclusion of legume cover crops means less CO_2 in the atmosphere, thus lowering the risk for global climate change.

Nitrogen is required in large amounts by plants. Soil has a limited amount of available nitrogen, thus making nitrogen the most limiting nutrient within the biomass production system. Overall, soils and the atmosphere only contain about 0.002% and 2% of global nitrogen, respectively. However, nitrogen can be fixed in symbiotic and industrial processes. Symbiotic processes are carried out in nodules located on roots typically found on legumes. Our study indicates that inclusion of legume cover crops in rotation

with cotton increases the amount of nitrogen stored in the soil, which can become available to a growing cotton crop. Our data also show that soil C/N ratios in this study are favorable with regard to mineralizing nitrogen that can be used to produce a cotton crop.

Mineralization is the breakdown of soil organic matter that converts organic forms of nitrogen into inorganic forms of nitrogen, while immobilization is the transformation of an inorganic nitrogen compound into organic nitrogen *(Varvel, 1994)*. Immobilization depends on the ratio of the total percent carbon to the total percent nitrogen, or C/N ratio. The C/N ratio determines whether immobilization or mineralization will occur. At a ratio of around 20-30, both immobilization and mineralization will occur. At any ratio below 20, only mineralization will occur, a process which supplies inorganic nitrogen for crop growth. Soils commonly range from 10 to 12 in C/N ratio. Based on the results from this experiment (Figure 1) all plots will experience mineralization, and supply some nitrogen to crop plants.

Conclusions

Based on results from this experiment, different crop rotations of cotton and cover crops affect concentrations of soil carbon and nitrogen, and C/N ratios. Plots without legume cover crop result in a lower amount of sequestered carbon. Planting cereals and corn in rotation with cotton provides an added impact on nitrogen, increasing soil nitrogen beyond legumes alone. Soils having a lower C/N ratio may provide more mineral nitrogen for crop growth via mineralization. This long-term study of soils at the *Old Rotation* demonstrates that management of crops through crop rotation impacts soil quality.

References

Drinkwater, L., E. P. Wagoner, and M. Sarrantonio. (2003). Legume-based cropping systems have reduced carbon and nitrogen losses, *Nature*: 396, 262-265.

Hubbs, M. D., D. W. Reeves, and C. C. Mitchell Jr. (1998). Measuring Soil Quality on the *Old Rotation*. Paper presented at the 21st Annual Southern Conservation Tillage Conference for Sustainable Agriculture, Southern Extension and Research Activity-Information Exchange Group 20 (SERA-IEG-20), Special Report 186.

Lal, R. (2004). Soil carbon sequestration to mitigate climate change. *Geoderma*: 123, 1-22.

Leeper, G. W. (1993). *Soil Science, an Introduction* (5th ed.). Melbourne: Melbourne University Press.

Mitchell, C. C., D. P. Delaney, and K. S. Balkcom. (2008). A historical summary of Alabama's *Old Rotation* (circa 1896): The world's oldest, continuous cotton experiment. *Agronomy Journal*: 100, 1493-1498.

Mitchell, C. C., and J. A. Entry. (1998). Soil C, N and crop yields in Alabama's long-term 'Old Rotation' cotton experiment. *Soil & Tillage Research*: 47, 331-338.

Varvel, G. E. (1994). Rotation and nitrogen fertilization effects on changes in soil carbon and nitrogen. *Agronomy Journal*: 86, 319-325.
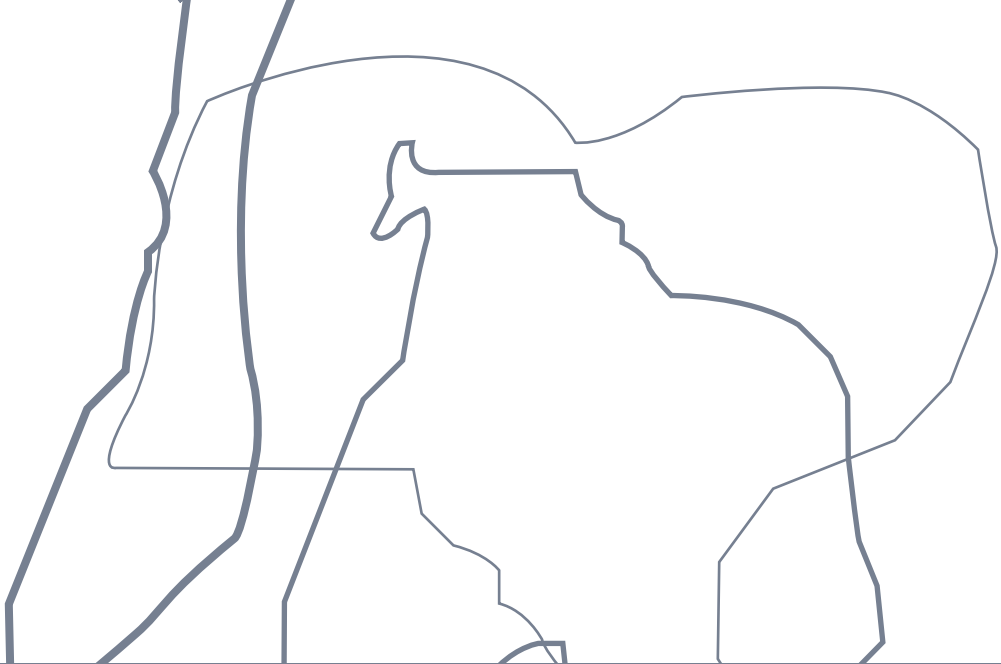
Plate Tectonic Implications of U-Pb Isotopic Age Dating of Detrital Zircons from the Caledonian Mountain System, Arctic Norway

Kristen McCall and Mark Steltenpohl

ABSTRACT

The precise location of the boundary (suture) separating the ancient continents of Laurentia (proto-Greenland and North America) and Baltica (proto-northern Europe) remains currently unknown by scientists. The focus of this study is to explore whether or not the Gullesfjord fault is that suture. All rocks surrounding this fault were previously thought to be 1.8 Ga (giga annums ~ billions of years ago), an age assignment that is strictly associated with Baltica. Key (*2010*), however, reported zircons dated from quartzites (metamorphosed sandstones) along the Gullesfjord fault to be younger than 1.1 Ga, which is an age associated with eastern Laurentia. Our study determined U-Pb isotopic abundances and ages on individual zircon crystals taken from other quartzite units surrounding the Gullesfjord Fault. These age dates are compared to the known age patterns of ancient proto-continents that evolved into Earth's continents today. Considered together with structural, lithological and field relationships, our results

distinguish sandstones that were deposited upon Laurentian continental basement (distinctive aged core rocks upon which a continent evolved) from those deposited upon Baltican basement. In addition to helping to constrain the position of the Baltican-Laurentia suture, our results also allowed us to document an older, previously unrecognized suture lying within Baltica.

INTRODUCTION

The northern Appalachian (U. S.) and Caledonian (U. K., E. Greenland, Norway, Sweden, and Svalbard) mountain systems formed during the middle Paleozoic period of Earth's history (around 450-390 Ma) when the ancient continents of Laurentia (proto-North America-Greenland) and Baltica (proto-northern Europe) collided and were sutured together to form the supercontinent Pangaea (*Roberts and Gee, 1985; Hatcher, 2010*). The ancient ocean basin previously separating Laurentia from Baltica, referred to as the Iapetus ocean (named after the Greek father of Atlantis

for whom the modern Atlantic Ocean was named), was subducted and destroyed in this process (*Rankin, 1975*).

Beach sands were deposited along the shores of these ancient continents (pre-collisional setting), precisely as we see along the east coast of the United States today. These sediments were lithified and later metamorphosed to form quartzites (Figure 1) under the intense heat and pressures associated with the ensuing continent-continent collision and formation of the Caledonian mountain belt.

The beach sands were derived from and deposited upon basement 'complexes' composed of plutonic igneous rocks (magmas that crystallized deep within the crust) that formed the very foundation upon which the ancient continents evolved (Figure 2). Importantly for our study, the igneous rocks contain the mineral zircon, which crystallized during the solidification of the magmas. Zircon is a durable mineral that can withstand the constant pounding of oceanic wave action and is found in
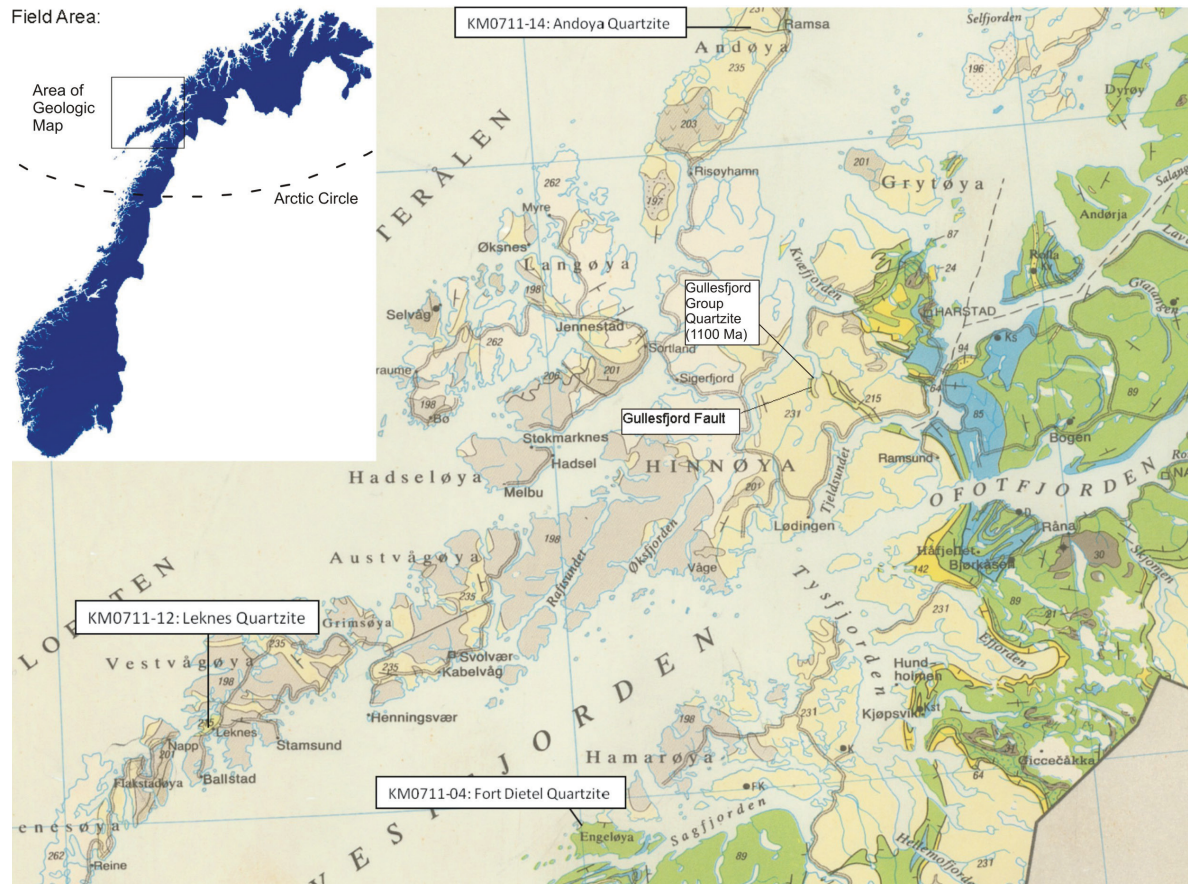
Figure 1. Geologic map portion of northern Norway (latitude 69° N) wherein field work was conducted with sample locations. Tan and brown colors represent Baltic basement, yellow is quartzite, and all other colors represent younger Caledonian and Iapetan rocks thrust eastward upon Baltica; map adapted from Sigmond et al. (1985). North is up on both maps. Scale for inset is 1" = 4575 km; scale for field area map is 1" = 25 km.

Figure 2. Cartoon diagram displaying provenances ages of Laurentian and Baltican source terrenes. Rocks of various colors display cross cutting relationships in the basement rocks that underlie the yellow quartzite unit, deposited at 0.7 Ga.

most sedimentary rocks (*Wilde et al., 2001*). U–Pb isotopic ages measured on the zircons, therefore, can be considered fingerprints that distinguish ancient continental land masses of particular age ranges from one another (*Anderson, 2005*). Baltica and Laurentia have distinctive age signatures of Ga 1.7 and 1.1 Ga, respectively (*Bergh et al., 2007*) (Figure 2). Hence zircons contained within the quartzites presently exposed in arctic Norway can be dated using U–Pb isotopic analyses to narrow down the position of the Iapetan suture, which

is not precisely known in the north Atlantic region.

GEOLOGICAL BACKGROUND AND HYPOTHESIS TO BE TESTED

The Lofoten-Vesteralen basement terrane in northern Norway (latitude 69° N: Figure 1) is dominated by 2.7 Ga Archean migmatite gneisses, 2.3 Ga supracrustals, and 1.8 to 1.7 Ga plutonic rocks (Figure 2) of predominately granitic composition (*Griffin et al., 1978*). Dates for the aforementioned granitic basement complexes surrounding the Gulles-

fjord fault in northern Norway (Figure 1) are well established (*Griffin et al., 1978; Corfu, 2004*). Key (2010) reported the surprising discovery of 1.1 Ga (Laurentian) detrital zircons from the basal quartzites of the Gullesfjord Group (Figure 1). These quartzites have a depositional contact directly upon the granites beneath them and they were previously thought to be the stratigraphic 'cover' to the Lofoten terrane, a known Baltican-age complex (*Griffin et al., 1978*). Further field and geochronological work in the region led to our hypothesis that the Gullesfjord fault could be the suture separating the proto-continents Laurentia and Baltica. To test this hypothesis, U–Pb isotopic age analysis was employed on detrital zircons from quartzite samples collected from three strategically determined areas around the Gullesfjord fault (Figure 1) where they are sandwiched between
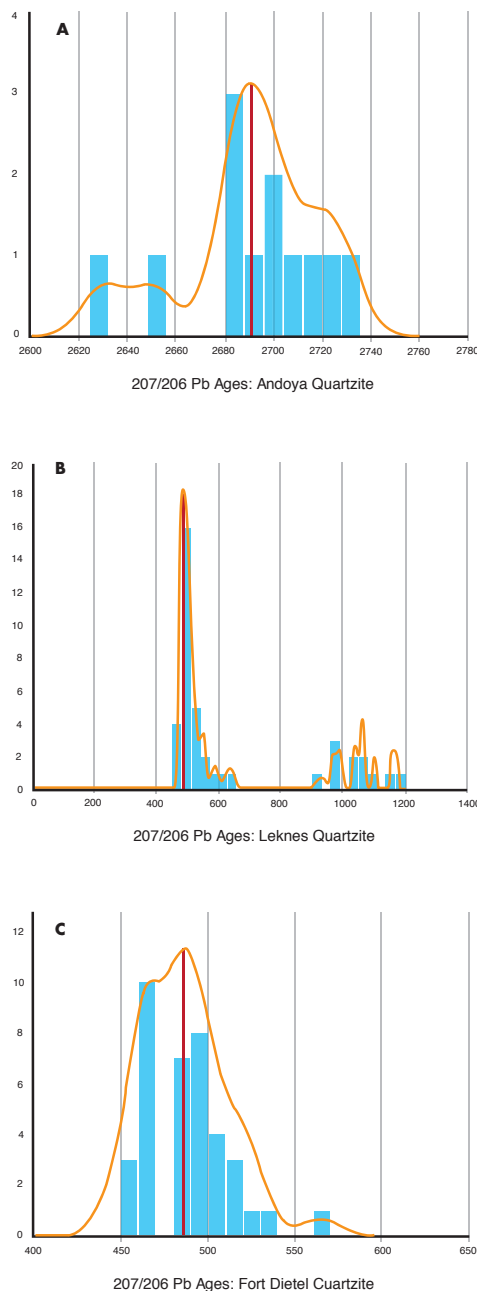
A

207/206 Pb Ages: Andoya Quartzite

B

207/206 Pb Ages: Leknes Quartzite

C

207/206 Pb Ages: Fort Dietel Cuartzite

Figure 3. Frequency Diagrams showing 207/206Pb ages generated through LA-ICPMS work. A. Andoya Quartzite. B. Leknes Quartzite. C. Fort Dietel Quartzite. All zircons ages depicted have <10% Central Discordance. Vertical Scale: number of zircons analyzed. Horizontal Scale: millions of years.

sheared and faulted plutonic basement rocks. Our analytical results, as shown below, indicate several surprising relationships between the three quartzites sampled.

METHODS

Five days of fieldwork were done to collect three samples and to characterize their field relationships. These samples include (sample number and rock unit): KM0711-

14, Andoya Quartzite; KM0711-12, Leknes Quartzite; and KM0711-04, Fort Dietel Quartzite.

The general methods used to prepare the samples at the University of Oslo for Laser Ablation Inductively Coupled Plasma Mass Spectroscopic (LA-ICPMS) analysis are as follows. The rock was placed in a rock crusher to achieve particles between sand and gravel size. A Retsch rock crusher was then used to bring the particles to <0.5 mm in size. A Wifley board (hydraulic gravity table) was used to separate out the fraction of the sample having the highest density by allowing water to run down a serrated table. The least dense fraction (lightest) particles floated off, leaving behind the medium density and heaviest fractions to be collected, which was good for our purposes because zircon has a relative high density of 4.7g/cm^3. Samples were then washed with alcohol and set in an oven to dry. The mineral grains were then passed through a magnetic separator to isolate heavy grains that were not magnetic (zircon) by extracting them in the sequence 0 to 0.4, 0.4 to 0.8 and 0.8 to 1.2 ammeters of magnetivity to ensure the highest probability of magnetic particle extraction. Heavy liquids and a separatory funnel were used to remove, by floating off, any particle having a density of <2.8 g/ml to ensure that mainly zircons remained in the sample to be analyzed. For each step, equipment had to be cleaned and re-assembled before use.

A binocular microscope and a very fine wetted brush were then used to individually pick out zircon crystals until more than 100 grains were segregated. They were then pipetted into a separate Petrie dish, stuck onto double sided tape, and placed on a piece of plastic dubbed a "puck." This puck was later polished and the zircon distribution pattern mapped as a guide to aid in the LA-ICPMS analyses. A standard digital camera and petrographic microscope were used to take images of the zircons. These images were then stitched together using Microsoft Word in order to provide a usable map from which we could locate the zircons to be analyzed. Isoplot (*Ludwig, 2003*), an Excel-based program, was then used to calculate U-Pb ratios yielded from raw LA-ICPMS data and to plot them on Concordia and frequency diagrams; only zircons with <10% central discordance (i.e., deviation from the standard Concordia diagram of Earth's age) were used in this analysis. The data presented are statistically

sound in accordance to the standards for U–Pb detrital zircon analysis of sedimentary provenances (*Anderson, 2005*).

SAMPLE DESCRIPTIONS

The first sample analyzed, the Andoya Quartzite (KM0711–14), was collected from near Ramsa on the island of Andoya (Figure 1). This quartzite unit is interlayered with marbles (metamorphosed limestones) that lithologically resemble those of the Gullesfjord Group, and both groups occur discontinuously along a similar stratigraphic level. The second sample (KM0711–12) is from the thrust-faulted (a horizontal fault that has undergone many kilometers of displacement) Leknes Group, a metasedimentary package that is sandwiched by granitic gneisses (see tan and brown units surrounding sample on Figure 1) of the Lofoten basement complex on the island of Vestvagoy. The third sample, the Fort Dietel quartzite (KM0711–04), was collected on Engeloya, 100 km south of Lofoten (Figure 1), where it is in structural contact with an undated igneous complex named the Rossoy basement (*Carter, 2000*).

DATA PRESENTATION AND INTERPRETATION

Detrital zircon LA–ICPMS analysis of the Andoya Quartzite, KM0711–14 reveals a dominant 2.6–2.7 Ga age peak (Figure 3A) without any 1.0 Ga signature, meaning that despite the lithological similarities with the Gullesfjord Group, the Andoya metasedimentary rocks are not derived from Laurentian basement. Furthermore, the lack of any 1.8 Ga detrital zircons can be grounds to rule out a Fennoscandian (Baltican) origin (Figure 4). Instead, the Andoya quartzite was most likely sourced from an older Archean-Paleoproterozoic (~ 3.0 to 2.6 Ga) source and then later incorporated within the Baltic basement wherein it presently resides. Paleoproterozoic cover sequences upon Archean basement within the West-Troms basement complex (Figure 4) are well documented on the island of Vanna located 250 km north of Andoya (*Bergh et al., 2007*). Our results suggest that these metasedimentary sequences are correlative, greatly expanding the known area of this basement complex (Figure 4). It also requires that a previously unrecognized, pre-1.8 Ga suture internal to Baltica separate the West Troms basement complex from Svecofinnia (Figure 4).

Detrital zircons extracted from the Leknes Group quartzite, KM0711-12, contain a strong 1.0 Ga age peak (10 of 28 grains: Figure 3B), matching that of the Gullesfjord Group metasediments. Therefore, we interpret the Leknes Group to be of exotic, or far-traveled, Laurentian heritage. This is supported by the only known source of detrital zircon age populations of ~1.1 Ga in Norway being the Sveconorwegian terrane (Figure 4), which lies hundreds of kilometers to the south. The Sveconorwegian terrane is the Norwegian age equivalent of the ancient Grenville Mountain belt in North America, which formed at 1.1 Ga. Sveconorwegian-age rocks are not reported anywhere in central and north Norway (Figure 4) and, therefore, the suture separating Laurentia and Baltica must lie very near this boundary. The predominant age peak (~73% of grains) at 490 Ma (Figure 3B) indicates a maximum age for deposition of the quartzite, indicating relatively fast deposition just prior to deep-crustal subduction and metamorphism during the formation of the Scandinavian Caledonides around 478 Ma (*Steltenpohl et al., 2011*). Agyei-Dwarko (2011) suggested that a lack of Archean zircons in Caledonian quartzites also points to a non-Baltican source, further supporting our interpretation that the Leknes Group quartzites are of an exotic Laurentian origin.

Detrital zircon analysis of the Fort Dietel Quartzite, KM0711-04 (Figure 1), indicates an age population peak at 488 Ma (Figure 3C), consistent with detritus from a volcanic/magmatic Island arc that formed in the ancient Iapetus ocean (Figure 5b). Island arcs are arcuate-shaped islands of coalescing volcanoes, like modern Sumatra, that form above subduction zones where tectonic plates collide and magmas rise to form volcanoes. This 488 Ma age peak is compatible with the age of volcanic rocks of the Grampian-Taconic arc terrane in the U. K., which comprises island arcs formed within the Iapetus ocean that were tectonically "beached" and sutured onto the Laurentian margin upon the closing of the ancient ocean basin, before their collision with Baltica. This age peak is well known in the very far-transported (1,000's of km) Iapetan terranes in the Caledonian Mountains both to the north and south of our study area (e.g., *Andresen and Steltenpohl, 1994; Barnes et al., 2007,* respectively).
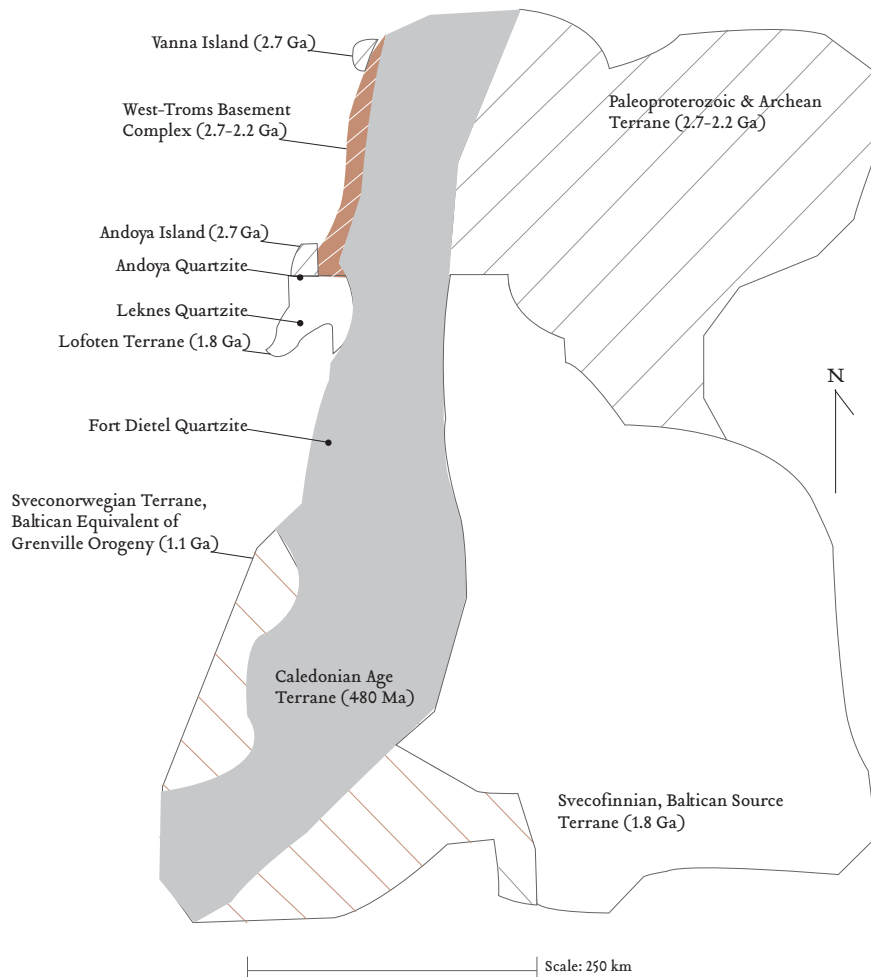

Figure 4. Cartoon map of northern Europe, which is underlain by the ancient Baltic proto-continent, collectively known as the "Fennoscandian Shield" or the Baltican Shield (after Corfu, 2004). Map depicts the known location of source terranes and their respective ages, sample collection localities, and the location of Vanna and Andoya islands.

CONCLUSIONS

Taken together, the data indicate that only the Andoya quartzite was deposited upon Baltic basement (West-Troms Basement Complex), whereas the remaining samples appear to have been deposited within far-travelled exotic terranes (Figure 5A). This relationship requires a previously unrecognized "Paleoproterozoic suture" in the study area (Figures 4 and 5). As a consequence to this suturing together of two proto-continental landmasses, mountains arose (a process referred to as "orogenesis"). This extinct Paleoproterozoic mountain belt was then beveled flat by a billion years of erosion, long before the Paleozoic (i.e., Caledonian) collision between Laurentia and Baltica. The Fort Dietel volcanic arc also formed prior to

the Caledonian orogeny, before being "beached" onto Baltica as it collided with Laurentia to consolidate the supercontinent Pangaea (Figure 5B). Baltican ages from units lying structurally below the Andoya basement-cover exposures implies that the Caledonian suture lies just above this horizon, but beneath the overlying Laurentian Leknes quartzite. Lastly, the work brings into question whether Laurentian granitic basement might also be locally preserved beneath some of the cover sequences preserved in arctic Norway. This hypothesis is testable through future isotopic age dating work, and could lead scientists to an even better understanding of where the suture lies that separates the two ancient proto-continents, Laurentia and Baltica, thus holding clues as to the geodynamic processes involved in the growth of Earth's continents.
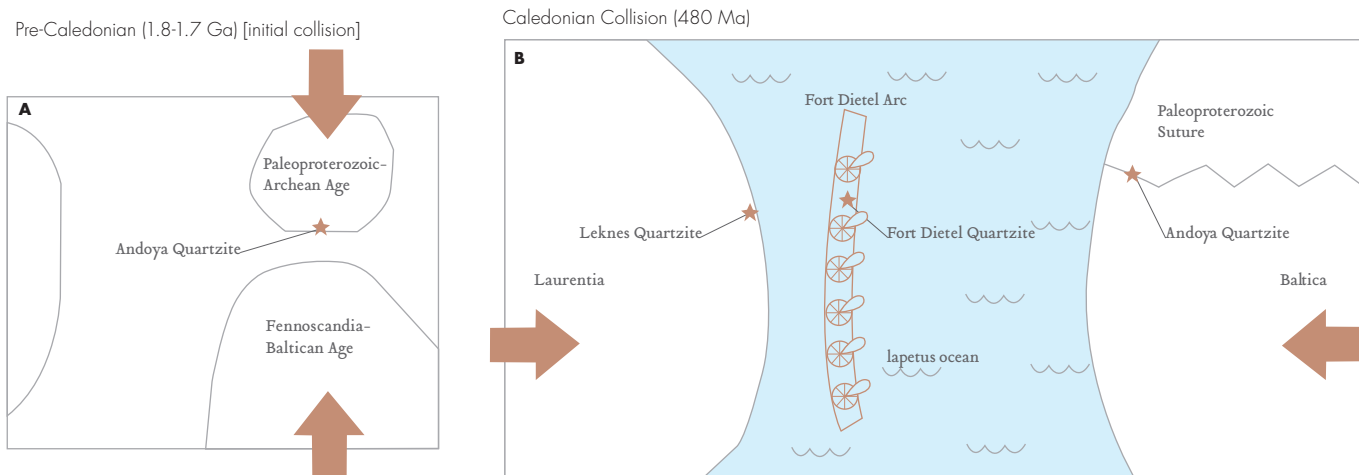
Pre-Caledonian (1.8-1.7 Ga) [initial collision]

Caledonian Collision (480 Ma)

Figure 5. Cartoon diagrams showing the evolution of the basement terranes preserved today in the arctic Caledonides. A. Paleoproterozoic provenance sources (2.7-2.2 Ga) that were once separated from Fennoscandia. B. The Fort Dietel volcanic arc lying within the Iapetus ocean prior to the Caledonian collision that sutured together Laurentia and Baltica around 450 to 390 million years ago. Stars indicate general position where sandstones examined in the current report were deposited.

REFERENCES CITED

Agyei-Dwarko, N. Y. (2011). The "basement" rocks in the Heggmovatn and Bodˉ areas: a Fennoscandian, Laurentian or suspect terrane? M.S. thesis, Department of Rocks and Geodynamics, Oslo, Norway: University of Oslo.

Anderson, T. (2005). Detrital zircons as tracers of sedimentary provenance: Limiting conditions from statistics and numerical simulation. Chemical Geology: 216 (3-4), 249-270.

Andresen, A. and M. G. Steltenpohl. (1994). Evidence for ophiolite obduction, terrane accretion, and polyorogenic evolution of the north Scandinavian Caledonides. Tectonophysics: 231 (1-3), 59-70.

Barnes, C. G., C. D. Frost, A. S. Yoshinobu, K. McArthur, M. A. Barnes, C. M. Allen, ÿ. Nordgulen and T. Prestvik. (2007). Timing of sedimentation, metamorphism, and plutonism in the Helgeland Nappe Complex, north-central Norwegian Caledonides. Geosphere: 3 (6), 683-703.

Bergh, S. G., K. Kullerud, F. Corfu, P. E. B. Armitage, B. Davidsen, H. W. Johansen, T. Pettersen and S. Knudsen. (2007). Low-grade sedimentary rocks on Vanna, North Norway: A new occurrence of a Palaeoproterozoic (2.4-2.2 Ga) cover succession in northern Fennoscandia. Norwegian Journal of Geology: 87 (3), 301-318, ISSN 029-196X.

Carter, B. T. (2000). Geological investigations in Steigen-Engelˉya, north-central Norway (68oN), and their significance for tectonic evolution. M.S. thesis, Department of Geology and Geography, Auburn, Alabama: Auburn University.

Corfu, F. (2004). U-Pb age, setting and tectonic significance of the Anorthosite-Mangerite-Charnockite-Granite Suite, Lofoten-VesterÅlen, Norway. Journal of Petrology: 45 (9), 1799-1819.

Griffin, W. L., P. N. Taylor, J. W. Hakkinen, K. S. Heier, I. K. Iden, E. J. Krogh, O. Malm, K. I. Olsen, D. E. Ormassen and E. Tveten. (1978). Archean and Proterozoic crustal evolution of Lofoten-VesterÅlen, North Norway. Journal of the Geological Society of London: 135 (6), 629-647.

Hatcher, R. D., Jr. (2010). The Appalachian orogen: A brief summary, in R. P. Tollo, M. J. Bartholomew, J. P. Hibbard and P. M. Karabinos (Eds.), From Rodinia to Pangea: The Lithotectonic Record of the Appalachian Region. Boulder, Colorado: Geological Society of America Memoir 206, 1-19.

Key, T. B. (2010). Structure and timing of the Austerfjord thrust and related shear zones, Hinnˉy, North Norway: Implications for late-stage Caledonian tectonic evolution: M.S. thesis, Department of Geology and Geography, Auburn, Alabama: Auburn University.

Ludwig, K. R. (2003). Isoplot 3.0, A Geochronological Toolkit for Microsoft Excel: Berkeley, California: Geochronology Center, Special Publication No. 4.

Rankin, D. W. (1975). The continental margin of eastern North America in the southern Appalachians: The opening and closing of the proto-Atlantic Ocean. American Journal of Science: 275-A, 298-336.

Roberts, D. and D. G. Gee. (1985). An introduction to the structure of the Scandinavian Caledonides, in D. G. Gee and B. A. Sturt (Eds.), The Caledonide Orogen- Scandinavia and Related Areas. Chichester, England: John Wiley and Sons, 55-68.

Sigmond, E. M., M. Gustavson, and D. Roberts. (1985). Berggrunnskart Over Norge, 1:1 Million Bedrock map of Norway. Norges Geologiske Undersˉkelse: Geological Survey of Norway.

Steltenpohl, M. G., G. Kassos, A. Andresen, E. F. Rehnstrˆm and W. E. Hames. (2011). Eclogitization and exhumation of Caledonian continental basement in Lofoten, North Norway. Geosphere: 7 (1), 202-218, doi: 10.1130/GES00573.1.

Wilde, S. A., J. W. Valley, W. H. Peck and C. M. Graham. (2001) Evidence from detrital zircons for the existence of continental crust and oceans on the Earth 4.4 Gyr ago. Nature: 409 (6817), 175-178.

STUDENT Author BIOS

John Shi

Senior in Economics (Yale); Research in Department of Pathobiology
Auburn University

John became interested in researching methods of solving mitochondrial disease after learning about the importance of mitochondria within the cellular network. As the "engine" of the cell, functioning mitochondria are crucial for proper cellular development. He plans to use the knowledge he has gained from his research in Dr. Pinkert's lab in tandem with his economics major to pursue a Ph.D./MBA joint degree.

Gabrielle Bates

Junior in Creative Writing, College of Liberal Arts

As an intern for the Auburn Office of University Writing, Gabrielle Bates was given the opportunity to look behind the scenes at some of the exciting opportunities offered to undergraduates by *AUJUS*. She wanted to write a feature article about the cover design because she was fascinated by the unique creative process and was eager to be a part of the *AUJUS* celebration of undergraduate writing. After graduating from Auburn University, Bates plans to get an MFA in Creative Writing and then pursue her long-term goals of traveling, publishing novels, and teaching English courses at the collegiate level.

Kelsey E. Herndon

Recent graduate in Anthropology, Department of Sociology, Anthropology and Social Work

Kelsey is currently serving as the Assistant Director of the Auburn University Bioanthropology Lab. She became interested in the study of ancient health because of her dedicated teachers who were willing to involve her in their own research projects. She plans to attend graduate school in the fall, where she will continue to investigate the health consequences of various transitional periods.

Kristen McCall

Senior in Geology, Department of Geology and Geography

Kristen became interested in Norwegian geology after taking Dr. Mark Steltenpohl's Physical and Structural Geology courses, and after her time as a research assistant in the Geology Department. After digging deeper into the cross sections of the fault systems she was digitizing, she wanted to learn more about the methods of figuring out how mountain belts such as the Caledonian system in Norway were formed, and so began her research. She plans to enter graduate school in fall 2012 to pursue a Master's degree that focuses on geochronology, metamorphism and the relation of each to larger scale tectonic events.

Hamilton Hastie Bryant III

Senior in Anthropology, Department of Sociology, Anthropology and Social Work

Hamilton became interested in archeology and anthropology as a child while looking for artifacts with his family along the Tensaw River in Baldwin County, Alabama. He has been working with Dr. Cottier on projects ranging from contract archaeology and public archaeology to instructing field schools and presenting research at academic conferences since he started at Auburn. He is interested in non-invasive archeological procedures. He wants to pursue a Ph.D. in Anthropological Archaeology with a focus on the prehistoric and historic periods of the southeastern United States.
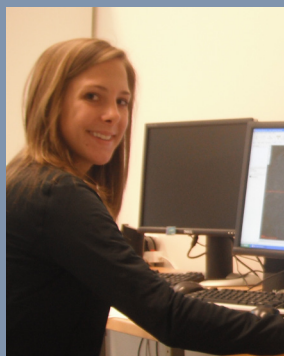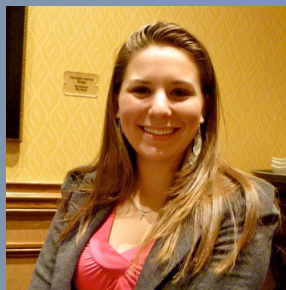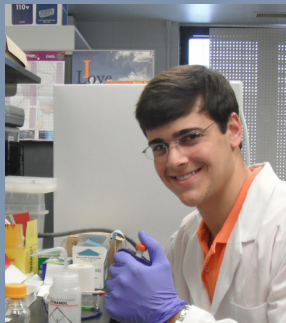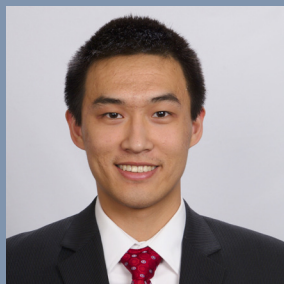
Bradley Lane Young

Junior in Biomedical Sciences, Department of Chemistry and Biochemistry

Brad chose to work with Dr. Zhan because he felt the work performed by the Zhan Research Group, which studies the power of lipid-based photovoltaic cells, could be the key to easing dependence on fossil fuels, a subject he is passionate about. He plans to graduate in May 2013 and study to be a doctor so that he can serve others. His ultimate career goal is to return to Alabama to set up a medical practice that would aim to make the world a better place.

J. Alyssa White

Sophomore in Anthropology and Spanish, Department of Sociology, Anthropology and Social Work

Alyssa became interested in the study of health through bioarchaeological analysis during her first year at Auburn, when she was inspired by her Introduction to Anthropology instructor to consider doing research in anthropology. She has since been actively pursuing questions of human health in the archaeological record. She plans to become a professional anthropologist and university professor at a research institute, and is currently refining her areas of interest and her skills as an anthropologist.

Rachel M. Perash

Senior in Anthropology, Department of Sociology, Anthropology and Social Work

Rachel came to Auburn with the hopes of becoming a marine archaeologist. After taking several major courses, she decided to switch to bioarchaeology and forensics. After graduating in December 2012, she plans to attend graduate school for a Master's and a Ph.D. After finishing her degrees, she would like to work in the field before ultimately becoming a professor.

Patrick Donnan

Sophomore in Physics and Music, Department of Physics

Patrick joined Dr. Robicheaux's lab after deciding he wanted to work in physics, and ended up working on the antihydrogen project, a project that has given him the chance to learn and work with many intricate physical concepts in atomic physics. He is trying to solve a mystery that is all around us: why is the known universe made of matter, and not antimatter? Patrick plans to go on to earn his Ph.D. in physics, complete a post-doctoral fellowship, and become a professor at a research university. He wants to mentor undergraduates in physics research one day.

Leffie Dailey

Recent graduate in Agronomy and Environmental Science, Department of Agronomy and Soils

Leffie is a resident of Macon, Georgia and has a strong family influence of farming. With a strong interest in soil preservation and environmental effects, Leffie was drawn to the opportunity to conduct research on the "Old Rotation." She appreciated the experience of applying concepts learned in the classroom as she worked alongside Dr. Wes Wood and Brenda Wood of the Auburn Agronomy Department. Leffie's immediate goal is to obtain a position in the environmental compliance field with a major corporation. She is also contemplating graduate school at the University of Georgia in environmental health.

Graphic Design Production Team

Devan Allegri
Junior, Fairhope, AL

Juliana Bone
Junior, Hazel Green, AL

Rachel Botts
Junior, Madison, AL

Nina Cotney
Senior, New Site, AL

Emily Edwards
Junior, Madison, AL

Jackie Fisher
Senior, Huntsville, AL

Mallory Godwin
Junior, Mobile, AL

Kara Hendley
Senior, Montgomery, AL

Kyle Humphrey
Senior, West Point, GA

Bailey Parkerson
Senior, Pelham, AL

Katherine Pottinger
Junior, Orlando, FL

Whitney Potts
Senior, Thorsby, AL

Gina Roberson
Junior, Phenix City, AL

Ashley Stephens
Senior, Woodstock, GA

Jennifer Thai
Senior, Huntsville, AL

Bethany Whitehead
Junior, Birmingham, AL

Cicily Williams
Senior, Bay Minette, AL

Lindsey Wilson
Junior, Madison, AL

AUJUS

Auburn University Journal of Undergraduate Scholarship

CALL FOR

SUBMISSIONS

The *Auburn University Journal of Undergraduate Scholarship* (*AUJUS*) is accepting scholarly articles for its Spring 2013 issue. *AUJUS* is a peer-reviewed journal that showcases the original research of Auburn University undergraduate students. Submissions will be accepted from April 2nd - September 4th, 2012

AUBURN
UNIVERSITY

AUJUS

Auburn University Journal of Undergraduate Scholarship

Undergraduate Research
Office of the Provost
209 Samford Hall
Auburn, AL 36849